# AFRL-PR-WP-TR-2001-2099

# IONICALLY CONDUCTING POLYMER ELECTROLYTES

BINOD KUMAR

UNIVERSITY OF DAYTON RESEARCH INSTITUTE
300 COLLEGE PARK
DAYTON, OH 45469-0170

JUNE 2001

FINAL REPORT FOR PERIOD 25 JUNE 1993 – 30 JUNE 2001

Approved for public release; distribution unlimited.

PROPULSION DIRECTORATE
AIR FORCE RESEARCH LABORATORY
AIR FORCE MATERIEL COMMAND
WRIGHT-PATTERSON AIR FORCE BASE, OH 45433-7251

20020213 085

# NOTICE

USING GOVERNMENT DRAWINGS, SPECIFICATIONS, OR OTHER DATA INCLUDED IN THIS DOCUMENT FOR ANY PURPOSE OTHER THAN GOVERNMENT PROCUREMENT DOES NOT IN ANY WAY OBLIGATE THE US GOVERNMENT. THE FACT THAT THE GOVERNMENT FORMULATED OR SUPPLIED THE DRAWINGS, SPECIFICATIONS, OR OTHER DATA DOES NOT LICENSE THE HOLDER OR ANY OTHER PERSON OR CORPORATION; OR CONVEY ANY RIGHTS OR PERMISSION TO MANUFACTURE, USE, OR SELL ANY PATENTED INVENTION THAT MAY RELATE TO THEM.

THIS REPORT IS RELEASABLE TO THE NATIONAL TECHNICAL INFORMATION SERVICE (NTIS). AT NTIS, IT WILL BE AVAILABLE TO THE GENERAL PUBLIC, INCLUDING FOREIGN NATIONS.

THIS TECHNICAL REPORT HAS BEEN REVIEWED AND IS APPROVED FOR PUBLICATION.

Lawrence G. Scanlon

LAWRENCE G. SCANLON
Project Scientist, Energy Storage
and Thermal Sciences Branch
Power Division

Brian G. Hager

BRIAN G. HAGER
Chief, Energy Storage and Thermal
Sciences Branch
Power Division
Propulsion Directorate

JoAnn L. Erno

JOANN L. ERNO, Lt Colonel, USAF
Deputy Chief
Power Division

Do not return copies of this report unless contractual obligations or notice on a specific document requires its return.

# REPORT DOCUMENTATION PAGE

*Form Approved*
*OMB No. 074-0188*

Public reporting burden for this collection of information is estimated to average 1 hour per response, including the time for reviewing instructions, searching existing data sources, gathering and maintaining the data needed, and completing and reviewing this collection of information. Send comments regarding this burden estimate or any other aspect of this collection of information, including suggestions for reducing this burden, to Washington Headquarters Services, Directorate for Information Operations and Reports, 1215 Jefferson Davis Highway, Suite 1204, Arlington, VA 22202-4302, and to the Office of Management and Budget, Paperwork Reduction Project (0704-0188), Washington, DC 20503.

| 1. AGENCY USE ONLY | 2. REPORT DATE | 3. REPORT TYPE AND DATES COVERED |
|---|---|---|
| | June 2001 | FINAL, 25 June 1993 – 30 June 2001 |

**4. TITLE AND SUBTITLE**

Ionically Conducting Polymer Electronics

**5. FUNDING NUMBERS**

C: F33615-93-C-2350
PE: 61102F
PR: 2303
TA: P4
WU: 00

**6. AUTHOR(S)**

Binod Kumar

**7. PERFORMING ORGANIZATION NAME(S) AND ADDRESS(ES)**

University of Dayton Research Institute
300 College Park
Dayton, OH 45469-0170

**8. PERFORMING ORGANIZATION REPORT NUMBER**

UDR-TR-2001-00091

**9. SPONSORING / MONITORING AGENCY NAME(S) AND ADDRESS(ES)**

Propulsion Directorate
Air Force Research Laboratory
Air Force Materiel Command
Wright Patterson AFB, OH 45433-7251
POC: Lawrence G. Scanlon Jr., AFRL/PRPS, (937) 255-7770

**10. SPONSORING / MONITORING AGENCY REPORT NUMBER**

AFRL-PR-WP-TR-2001-2099

**11. SUPPLEMENTARY NOTES**

**12a. DISTRIBUTION / AVAILABILITY STATEMENT**

Approved for public release, distribution unlimited.

**12b. DISTRIBUTION CODE**

**13. ABSTRACT** ***(Maximum 200 Words)***

This report presents an investigation on the development of composite electrolytes for lithium batteries. The investigation covers a diverse range of composite electrolyte compositions and reveals that the incorporation of a ceramic component in a polymer matrix leads to enhanced conductivity. The conductivity enhancement depends upon the weight fraction of the ceramic phase, annealing parameters, nature of polymer-ceramic system, and temperature. The roles of ceramic additives are to depress the poly(ethylene oxide) (PEO) melting temperature and retard kinetics of its crystallization. A resistivity relaxation or conductivity enhancement below the melting temperature of PEO occurs, which appears to be a characteristic of these electrolytes and related to an interaction of dipoles associated with polymer chain and ceramic particles.

**14. SUBJECT TERMS**

Polymer electrolytes, ceramic additives, ionic conductivity, and dipole-dipole interaction

**15. NUMBER OF PAGES** 76

**16. PRICE CODE**

| 17. SECURITY CLASSIFICATION OF REPORT | 18. SECURITY CLASSIFICATION OF THIS PAGE | 19. SECURITY CLASSIFICATION OF ABSTRACT | 20. LIMITATION OF ABSTRACT |
|---|---|---|---|
| UNCLASSIFIED | UNCLASSIFIED | UNCLASSIFIED | SAR |

Standard Form 298 (Rev. 2-89) (EG)
Prescribed by ANSI Std. 239-18
Designed using Perform Pro. WHS/DIOR, Oct 94

## *TABLE OF CONTENTS*


| SECTION | | PAGE |
|---|---|---|
| | LIST OF FIGURES | v |
| | LIST OF TABLES | vii |
| | ACKNOWLEDGMENTS | viii |
| 1 | INTRODUCTION | 1 |
| 2 | EXPERIMENTAL | 6 |
| | 2.1 ELECTROLYTE FILM PREPARATION | 6 |
| | 2.2 CONDUCTIVITY MEASUREMENT | 7 |
| | 2.2.1 Theory | 7 |
| | 2.2.2 Procedure | 9 |
| | 2.2.3 Conductivity Computation | 11 |
| | 2.3 DIFFERENTIAL SCANNING CALORIMETRY | 12 |
| | 2.4 INFRARED ABSORPTION SPECTROSCOPY | 12 |
| | 2.5 MECHANICAL STRETCHING | 12 |
| 3 | RESULTS AND DISCUSSION | 14 |
| | 3.1 BACKGROUND | 14 |
| | 3.2 EFFECTS OF COMPOSITION | 14 |
| | 3.2.1 PEO:$LiBF_4$ (8:1)-$TiO_2$ (20 wt%, 21 nm) | 14 |
| | 3.2.2 PEO:$LiBF_4$ (8:1)-MgO (10 wt%, 15 nm) | 16 |
| | 3.2.3 PEO:$LiBF_4$ (8:1)-MgO (20 wt%) | 18 |
| | 3.2.4 PEO:$LiBF_4$ (8:1)-MgO (30 wt%) | 20 |
| | 3.2.5 PEO:$LiBF_4$ (8:1)-$BaTiO_3$ System | 22 |
| | 3.2.6 Relative Comparison of Composite Electrolytes | 25 |
| | 3.3 CONDUCTIVITY RELAXATION | 25 |
| | 3.4 EFFECT OF PARTICLE SIZE | 31 |

## *TABLE OF CONTENTS (Concluded)*


| SECTION | | PAGE |
|---|---|---|
| | 3.4.1 Conductivity as Influenced by the Size of Ceramic Additive | 31 |
| | 3.4.1.1 PEO:$LiBF_4$ (8:1)-MgO (10 wt%) Materials | 31 |
| | 3.4.1.2 PEO:$LiBF_4$ (8:1)-$BaTiO_3$ (20 wt%) Materials | 33 |
| | 3.4.2 Physical Properties of MgO and $BaTiO_3$ Powders | 35 |
| | 3.4.3 Crystalline Characteristics of the Polymer Phase | 36 |
| | 3.4.4 The Dominant Variable | 37 |
| | 3.5 CRYSTALLINE ⇔ AMORPHOUS TRANSITION | 39 |
| | 3.5.1 Differential Scanning Calorimetry and Thermogravimetric Analysis Measurements | 40 |
| | 3.5.2 Effect of $Al_2O_3$ Particle Size on Crystalline ⇔ Amorphous Transition | 43 |
| | 3.6 DIPOLES AND THEIR POSSIBLE EFFECTS | 46 |
| | 3.6.1 Conductivity Data of the Composite Electrolyte (without the dc field) | 48 |
| | 3.6.2 Effects of the dc Field | 48 |
| | 3.6.3 Effect of Mechanical Stretching | 50 |
| | 3.6.4 Infrared Absorption Spectroscopy | 54 |
| 4 | SUMMARY AND CONCLUSIONS | 58 |
| 5 | REFERENCES | 61 |
| | LIST OF SYMBOLS, ABBREVIATIONS, AND ACRONYMS | 63 |

## *LIST OF FIGURES*


| FIGURE | | PAGE |
|---|---|---|
| 1 | Equivalent Circuit and Complex Impedance Plots of Solid Electrolytes..... | 8 |
| 2 | A Typical Complex Impedance Plot for a Real, Polymer Electrolyte/ Blocking Electrode Cell ..... | 9 |
| 3 | Design and Dimensions of Electrodes used for Conductivity Measurement of Composite Electrolytes (Not to Scale, 316SS Material)..... | 10 |
| 4 | Teflon Cell Body Design and Dimensions (Not to Scale, Teflon Material) .. | 11 |
| 5 | Mechanical Device for Stretching of the Composite Electrolyte Film ..... | 13 |
| 6 | Temperature Dependence of Conductivity of PEO:$LiBF_4$ (8:1)-$TiO_2$ (20 wt%, 21 nm) Composite Electrolyte Annealed at 60 and 100 °C..... | 15 |
| 7 | Temperature Dependence of Conductivity of PEO:$LiBF_4$ (8:1)-MgO (10 wt%, 15 nm)..... | 17 |
| 8 | Temperature Dependence of Conductivity of PEO:$LiBF_4$ (8:1)-MgO (20 wt%, 15 nm) During Heating and Cooling Scans..... | 19 |
| 9 | Temperature dependence of Conductivity of PEO:$LiBF_4$ (8:1)-MgO (30 wt%, 15 nm) Electrolyte Subjected to Three Heat Treatments..... | 21 |
| 10 | Temperature Dependence of Conductivity of PEO:$LiBF_4$ (8:1)-$BaTiO_3$ (10 wt%) Annealed at 100 and 60 °C for 2 and 90 hours, Respectively..... | 23 |
| 11 | Temperature Dependence of Conductivity of PEO:$LiBF_4$ (8:1)-MgO: $BaTiO_3$ (18.5 wt% and 1.5 wt%, Respectively)..... | 24 |
| 12 | Conductivity Relaxation of the PEO:$LiBF_4$-$ZrO_2$ (30 wt%) at 20 °C, [O]:[Li] = 12.64:1..... | 29 |
| 13 | Conductivity Relaxation at 28°C in PEO:$LiBF_4$ (12.64:1)-$ZrO_2$ (30 wt%). | 30 |
| 14 | Schematic of Conductivity Relaxation Regions in Polymer-Ceramic Composite Electrolytes ..... | 30 |
| 15 | Temperature Dependence of Conductivity of PEO:$LiBF_4$ (8:1) Electrolyte Doped with Nano- and Micro-size MgO..... | 32 |
| 16 | Temperature Dependence of Conductivity of PEO:$LiBF_4$ (8:1) Electrolyte Doped with Nano- and Micro-size $BaTiO_3$..... | 34 |
| 17 | DSC Data of PEO:$LiBF_4$ (8:1)-MgO (10 wt%, Micro-size) Specimen Aged at 25 °C for Various Times ..... | 36 |

## *LIST OF FIGURES (Concluded)*


| FIGURE | | PAGE |
|---|---|---|
| 18 | Schematic Representation of a Polymer Chain Segment and MgO Particle Interaction | 38 |
| 19 | DSC Scans of PEO:$LiBF_4$ (8:1)-MgO (20 wt%, 24 nm) Specimen Subjected to a Thermal Treatment at 100 °C for 1 Hour | 41 |
| 20 | TGA Scan of PEO in the 0 to 1000°C Range Showing a Decomposition Peak Temperature at 378.6 °C | 42 |
| 21 | DSC Scans of PEO:$LiBF_4$ (8:1)-$Al_2O_3$ (20 wt%, 24 nm) Specimen | 43 |
| 22 | DSC Scans of PEO:$LiBF_4$ (8:1)-$Al_2O_3$ (20 wt%, 10 μm) Specimen | 44 |
| 23 | DSC Scans of PEO:$LiBF_4$ (8:1)-$Al_2O_3$ (20 wt%, 100 μm) Specimen | 44 |
| 24 | Conductivity of PEO:$LiBF_4$ (8:1)-MgO (10 wt%) Before and After Application of dc Field | 49 |
| 25 | AC Impedance Spectra of PEO:$LiCF_3SO_3$ (8:1)-MgO (10 wt%) Films | 52 |
| 26 | Temperature Dependence of Conductivity of PEO:$LiCF_3SO_3$ (8:1)-MgO (10 wt%) Films after Annealing at 60 °C for 132 Hours | 53 |
| 27 | IR Absorption Spectra of PEO:$LiBF_4$ (8:1) Complex and PEO:$LiBF_4$ (8:1)-MgO (20 wt%) Composite Films | 55 |
| 28 | IR Absorption Spectra of PEO:$LiBF_4$ (8:1)-MgO (20 wt%) Composite Electrolyte | 55 |

## *LIST OF TABLES*


| TABLE | | PAGE |
|---|---|---|
| 1 | Composition of Materials: Effect of Variables | 26 |
| 2 | Physical Properties of MgO and $BaTiO_3$ | 35 |
| 3 | DSC Parameters as Influenced by Thermal Treatments | 41 |
| 4 | Particle Size Effects on Crystallization of PEO:$LiBF_4$ (8:1)-$Al_2O_3$ (20 wt%) Material | 45 |
| 5 | Infrared Bands and Assignments in PEO:$LiBF_4$:MgO Complexes (2000 to 400 $cm^{-1}$) | 56 |

## *ACKNOWLEDGMENTS*

The work documented in this report was performed by the University of Dayton Research Institute between 25 June 1993 and 30 June 2001, for the Air Force Research Laboratory's Energy Storage and Thermal Sciences Branch (AFRL/PRPS) at Wright-Patterson Air Force Base, Ohio, under Contract F33615-93-C-2350. Experimental measurements were conducted by Mrs. L. Lucente, Mr. A. E. Turner, and Dr. S. J. Rodrigues. The author also expresses his appreciation to Mr. R. A. Marsh for his support during initiation and tenure of this program.

# *SECTION 1*
# *INTRODUCTION*

A variety of dielectric materials, such as polymers, glasses, ceramics, and their combinations, may be useful as solid electrolytes for lithium rechargeable batteries. Among these materials, polymers have received considerable attention in the last two decades because of their low density, manufacturability, and capacity to accommodate volume change as compared to a true rigid inorganic solid electrolyte. The subject of polymer electrolytes has been extensively covered by review papers and a monograph [1, 2]. Inorganic solids and glasses as electrolytes have also received significant attention [3, 4], but to a lesser degree.

A material containing polymer and ceramic components is identified as a polymer-ceramic composite. This composite material, with significant lithium ion conductivity, thus becomes a subset of solid electrolytes and has received considerable attention. For example, three review papers [5-7] have been published on the topic in the last seven years.

Because of its popularity, poly(ethylene oxide) (PEO) has been the polymer of choice in the polymer component for many studies; however, the choice of ceramic component has been arbitrary and diverse. It may be argued that a suitable matrix should facilitate the transport of lithium ions, which narrows the choice of the polymer component. But, what criteria should be used in selecting a ceramic component? This question was addressed in an earlier publication [5]. In general, the ceramic component of polymer-ceramic composite electrolytes can be classified into two categories: active and passive. The active category is comprised of materials such as $Li_3N$ and $LiAlO_2$. Due to the presence of lithium ions, these materials participate in the conduction process. The passive category is comprised of materials such as

$Al_2O_3$, $SiO_2$, etc., which do not participate in the conduction process. The choice between active and passive categories has been quite arbitrary.

The PEO is obtained by polymerization of monomer ethylene oxide ($CH_2CH_2O$) by a ring opening mechanism. The molecules of the $CH_2CH_2O$ monomer are highly strained and possess a triangular structure with melting and boiling points of -113 and 10.7 °C, respectively. The choice of polymerization initiators allows the preparation of polymers with a wide range of molecular weights (20,000 to 8,000,000). The PEO is a linear polymer and the regularity of polymerized units allows a high degree of crystallinity—in some cases, up to 85 percent. The melting point of PEO is 65 °C; however, the liquid ⇔ solid transition at the melting point is sluggish because of the high viscosity of the liquid phase. Commercially available PEO is thus a mixture of crystalline and amorphous states, and the ratio of crystalline to amorphous states may change depending upon the processing variables and impurities.

Ionic conduction in high-molecular weight PEO doped with sodium and potassium salts was reported by Wright [8]. However, the technological implications of PEO-based electrolytes were suggested by Armand and coworkers [9]. After this publication, significant research activities on PEO-based electrolytes began around the world [1, 2, 6]. The combination of PEO and lithium salts provides polymer-like materials that are electrochemically stable and can be processed in thin film form on a commercial scale.

A solid, composite electrolyte containing both polymer and ceramic components is the primary focus of the work highlighted in this report. The polymer component serves as a matrix in which the ceramic component is dispersed and also facilitates processing of the material into

thin films. As stated earlier, a suitable matrix should facilitate the transport of lithium ions and also provide electrochemical stability, justifying the use of PEO.

In general, the polymer component of a PEO-based composite electrolyte is a mixture of crystalline and amorphous states, the ratio of which depends to a great extent on the composition of the electrolyte, temperature, and thermal history. A predominance of the amorphous state is desirable if one is interested in a material with high conductivity. The fast ionic transport takes place in the amorphous phase; the conductivity is about two to three orders of magnitude greater as compared to the crystalline phase [10]. It has also been reported that the crystalline $\Leftrightarrow$ amorphous transition is sluggish which is also why the conductivity is dependent on thermal history [7]. The transition also takes place around ambient temperature and within the operating temperature range of lithium batteries.

An analysis of a broader range of composite electrolytes reveals that the incorporation of both active and passive categories in the ceramic component in a polymer matrix leads to enhancements in conductivity, cationic transport number, and electrode electrolyte interfacial stability [7].

The conductivity enhancement varies depending upon the fraction of ceramic phase, annealing parameters, polymer-ceramic systems, and temperature. In some polymer-ceramic systems, an increase of approximately four orders of magnitude in conductivity around and below ambient temperature has been achieved. The enhancement is accompanied by a reduction in the temperature dependence of conductivity. Analyses of experimental conductivity data of composite electrolytes strongly suggest that a new transport mechanism evolves.

The fact that polymer chain motion contributes to the transport of lithium ions in the polymer electrolytes also has a deleterious effect on the lithium transport number. The chain motion also facilitates the transport of anionic species; thus, measured conductivity includes contributions from both species. Some polymer electrolytes have a lithium transport number as small as 0.3. Why would the large size and heavy mass of the anionic groups compared to lithium have a transport number around 0.7? The literature on polymer electrolytes has not directly addressed this question. In a truly solid electrolyte consisting of similar cationic and anionic species, this behavior is improbable because the vibrational frequency and jump probability for cationic species would be much greater than for the anionic species. A possible answer to the question is related to the coupling phenomenon. It is conceivable that the anionic species is more coupled to the polymeric structure than the cationic species, which may account for its higher transport number. The vibrational frequencies and motion of large anionic species and polymer chains are expected to be more in phase than those of cationic species and polymer chains. Ceramic additives decouple structural and electrical relaxations by increasing the glass transition temperature. A number of experimental results on the lithium ion transport number support this hypothesis.

In a lithium rechargeable battery, the electrode-electrolyte interface is of critical importance. The extreme reactivity of the lithium metal (either electrode or dendrite), makes most of the polymer electrolytes unstable. In particular, impurities such as oxygen and water tend to accelerate the lithium passivation mechanism. A few ceramic materials (MgO, CaO, $Si_3N_4$) have positive free energy of reaction with lithium and should affect the formation, growth, and passivation of metallic lithium dendrite at the electrode-electrolyte interface.

When this program began, the state of understanding of polymer-ceramic composite electrolytes was very limited [5]. During the tenure of this program, a number of critical issues such as compositional effects, influence of ceramic particle size, polymer-ceramic complex formation, and roles of crystalline ⇔ amorphous transition have been identified, investigated, and explained. The investigation of these issues and their detailed analyses will be discussed in subsequent sections.

# *SECTION 2*
# *EXPERIMENTAL*

## 2.1 ELECTROLYTE FILM PREPARATION

A number of processing techniques may be used to obtain film and bulk specimens of polymer-ceramic composite electrolytes for laboratory evaluations. The most convenient one is the blend and press technique in which the polymer, lithium salt, and ceramic components are mixed in a predetermined proportion, ground in a mortar and pestle, hot pressed into pellet form, and then rolled into films of desired thickness. The processing parameters such as compacting pressure, temperature, time, and rolling conditions depend upon compositions. A range of materials covering a wide concentration of ceramic component in a polymer matrix can be obtained by this technique [11]. The second technique is melt casting which is a modified version of the blend and press technique. In this technique, a mixture of PEO, lithium salt, and ceramic is thoroughly mixed in the dry state, melted, homogenized in the temperature range of 175 to 200 °C, and subsequently cast either in film form or bulk material. The third technique is solvent casting, in which a solid ceramic phase is dispersed in a solution of polymer and lithium salt. The homogenized colloidal solution is then cast into a mold to obtain films of varying thicknesses [12]. These three techniques and their variations can provide films covering a variety of polymers and diverse ceramic components.

This report covers materials prepared by the second (melt cast) and third (solvent cast) techniques. The specimens and relevant data in the text will be identified accordingly.

## 2.2 CONDUCTIVITY MEASUREMENT

### 2.2.1 Theory

The most popular approach to measure the conductivity of an ionically conductive polymer is the alternating current (ac) method. The method can employ either blocking (stainless steel alloy) or nonblocking (lithium metal) electrodes. A sinusoidal voltage is applied to a cell and the current passing through the cell is determined. Two parameters are required to relate current flowing across the cell to the applied voltage. The first parameter is the hindrance to the flow of charge and is equal to the ratio of the voltage and current maxima, $V_{max}/I_{max}$, and is analogous to the resistance in direct current (dc) measurement. The second parameter, $\theta$, is the phase difference between the voltage and current. The combination of these two parameters is the impedance, Z, of the cell.

The polymer electrolyte in a blocking electrode configuration can be modeled as resistor and capacitor elements connected in parallel such as shown in Figure 1(a). The theoretical complex impedance plot of the equivalent circuit of Figure 1(a) is represented by Figure 1(b). It should be noted that a plot of real ($Z'$) and imaginary ($Z''$) parts of the impedance as a function of frequency yields a single semicircle whose diameter on the $Z'$ axis is equivalent to the resistance, R, of the polymer electrolyte. The intersections of the semicircle with the $Z'$ axis correspond to the highest ($Z' = 0$) and lowest ($Z'' = R$) frequencies. Thus, R can be approximated as dc resistance.

The experimental complex impedance plot of polymer electrolytes, Figure 2, deviates slightly from the theoretical plot of Figure 1(b). In reality, the complex impedance plots of polymer

electrolytes are broadened and electrode spikes are nonvertical. The discrepancy between the theory and practice has been discussed in the literature [13].

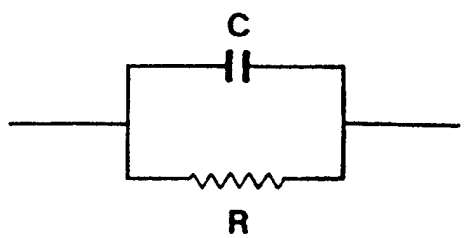


(a)

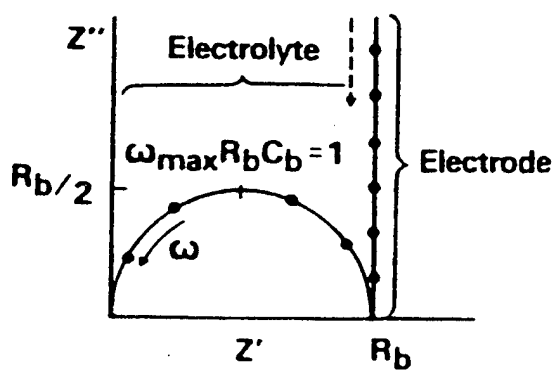


(b)

Figure 1. Equivalent Circuit and Complex Impedance Plots of Solid Electrolytes
(a) A Polymer Electrolyte in a Blocking Electrode Configuration; and
(b) Impedance Plot of Resistor, R, and Capacitor, C, Showing Electrolyte and Electrode Contributions

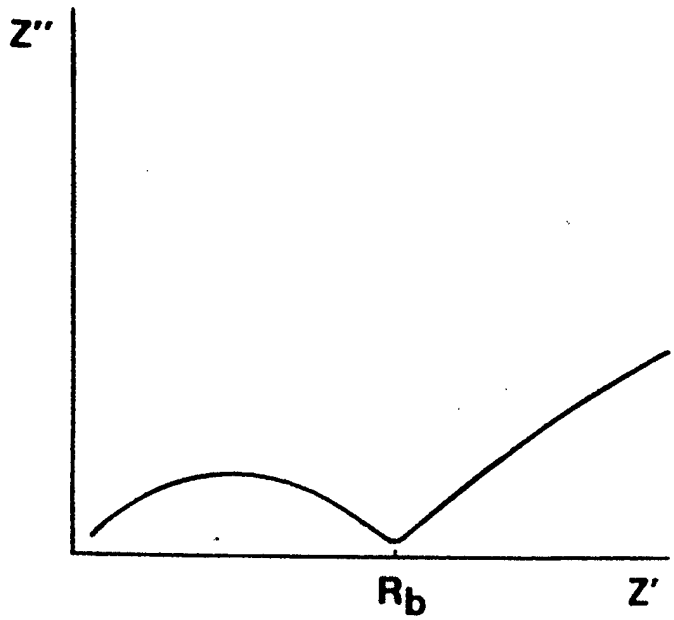


Figure 2. A Typical Complex Impedance Plot for a Real, Polymer Electrolyte/Blocking Electrode Cell

### 2.2.2 Procedure

The ac impedance measurements of composite electrolyte films were carried out using an EG&G Impedance Spectrometer Model 398 in the frequency range of 0.1 to 100 kHz. The design and dimensions of electrodes are shown in Figure 3. The electrolyte film is sandwiched between the electrodes which are enclosed in a Teflon cell body as shown in Figure 4. The assembled cell is subsequently contained in a glass vessel with electrical outlets, which are connected to the impedance spectrometer. The assembly of a cell, its containment in the glass vessel, and preliminary impedance measurement are conducted in the dry box, which is maintained at about 25 °C with a moisture and oxygen content of less than 1 ppm in each. Once it is established that the film quality is acceptable, the glass vessel with the cell is subsequently transferred to a Tenny Model $TUJ_r$ environmental chamber. The temperature dependence of conductivity data are obtained in this environmental chamber.

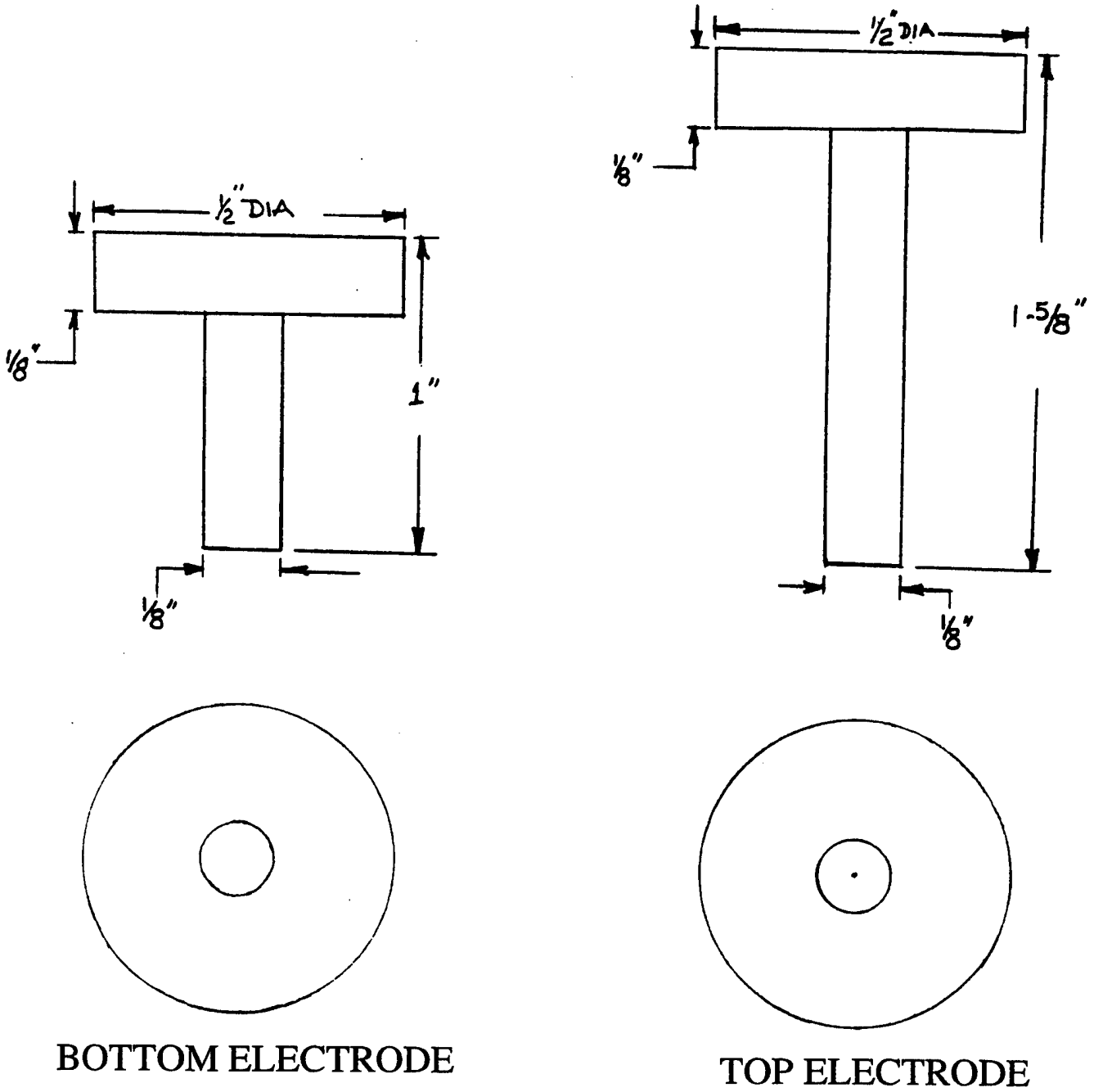


Figure 3. Design and Dimensions of Electrodes used for Conductivity Measurement of Composite Electrolytes (Not to Scale, 316SS Material)

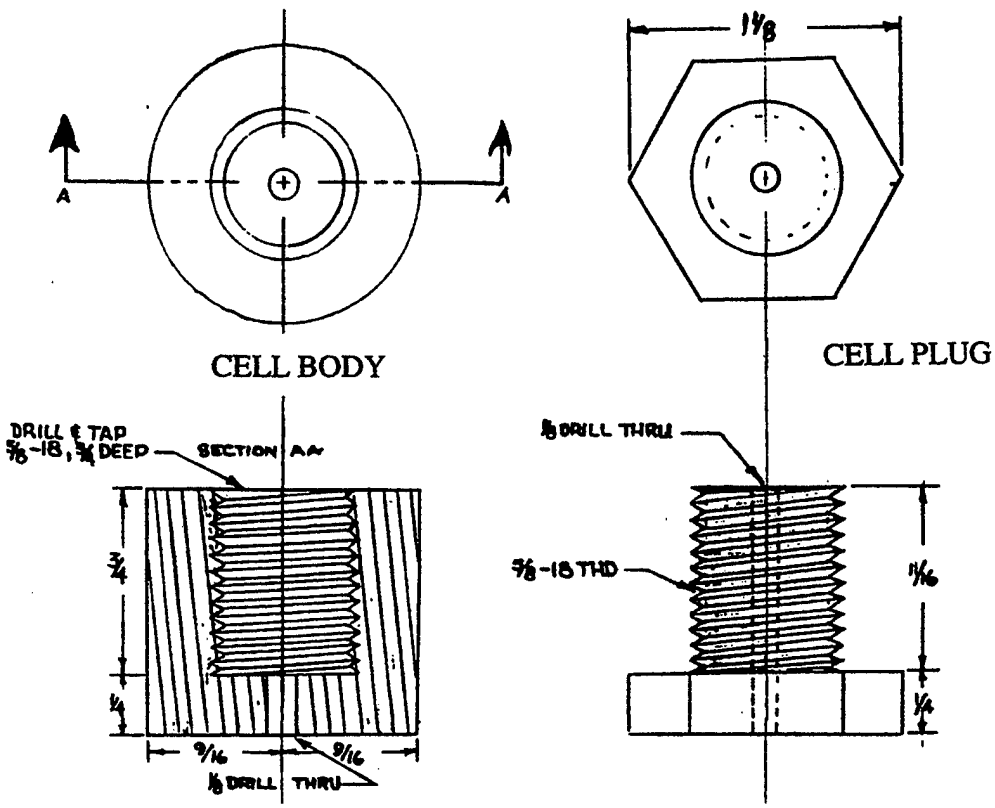


Figure 4. Teflon Cell Body Design and Dimensions (Not to Scale, Teflon Material)

### 2.2.3 Conductivity Computation

The conductivity, σ, is calculated from the resistance, R, of the electrolyte as determined from the impedance measurement, Figures 1(b) and 2, by using:

$$\sigma = \frac{t}{AR} \tag{1}$$

where $t$ = thickness of the film in cm

$A$ = area of the film in $cm^2$

The conductivity data are presented by a plot of $\log_{10}\sigma$ versus 1000/T(K). Sometimes the activation energy for the transport process, ΔH, is also obtained from the plot and reported.

## 2.3 DIFFERENTIAL SCANNING CALORIMETRY

Differential scanning calorimetry (DSC) measurements of composite electrolyte specimens were carried out using a TA Instruments Model 2910 at varying heating rates of 0.5 to 10 °C $min^{-1}$ between 0 to 200 °C under argon atmosphere. Pure indium and tin were used for temperature and enthalpy calibration of the instrument. Approximately 9 mg of the film specimen was used.

## 2.4 INFRARED ABSORPTION SPECTROSCOPY

Infrared (IR) vibrational spectra were obtained on the films using a Nicolet Fourier Transform Infrared (FTIR) spectrometer in 4000 to 500 $cm^{-1}$.

## 2.5 MECHANICAL STRETCHING

A mechanical stretcher was designed and assembled to investigate effects of mechanical stress and resulting elongation of the composite electrolyte on conductivity. The stretcher is shown in Figure 5 which basically consists of a two-prong clamp with two additional tubing clamps fitted at the lips of the two-prong clamp. The tubing clamps hold the film while the stretching stress is applied by unscrewing the two-prong clamp. The film was unannealed, heated to about 55 °C ± 5 °C by a blow drier while it was stretched.

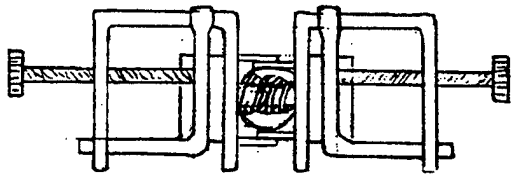

(a)

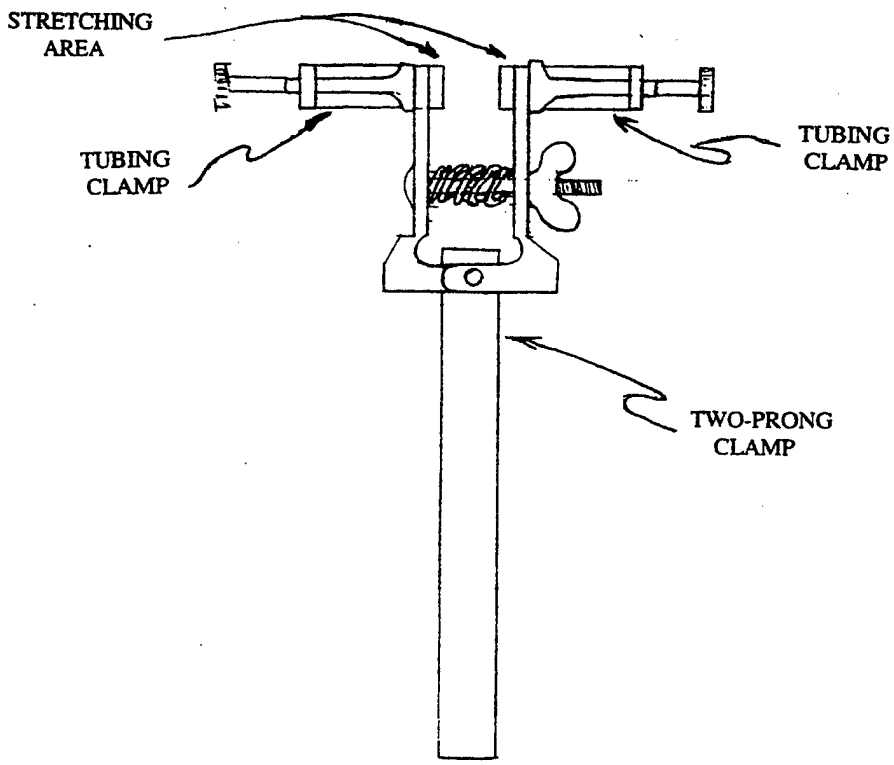


(b)

Figure 5. Mechanical Device for Stretching of the Composite Electrolyte Film
(a) Top View and (b) Side View

## *SECTION 3*
## *RESULTS AND DISCUSSION*

### 3.1 BACKGROUND

Soon after the program began, it became evident that the polymer-ceramic composite system is a complex system and a number of variables must be considered to explain the properties and performance of the composite electrolyte systems. The ionic conductivity, $\sigma$, of composite electrolytes is dependent upon a large number of variables such as the characteristics (chemistry, size, and volume fraction) of the ceramic component, thermalization (heating rates, hold time, cycling, etc.) parameters, properties of polymer components, degree of reactivity between polymer and ceramic components, and temperature. The thermalization step is basically a processing issue. Thus, it is apparent that the properties of a given polymer-ceramic composite electrolyte depend not only on the composition of the film but also on how it has been processed. This section has been accordingly structured. The subsections deal with the effects of composition, ceramic particle size, processing parameters, and related attributes.

### 3.2 EFFECTS OF COMPOSITION

#### 3.2.1 PEO:$LiBF_4$ (8:1)-$TiO_2$ (20 wt%, 21 nm)

The temperature dependence of conductivities of PEO:$LiBF_4$-$TiO_2$ (20 wt%) films obtained by the solution cast process and subjected to various heat treatments are shown in Figure 6. A cell containing the composite electrolyte in blocking electrode configuration (SS/film/SS) was subjected to various heat treatments at 60 and 100 °C. The electrolyte shows a conspicuous effect of heat treatment on conductivity over the temperature range of 0 to 100 °C. However,

the phenomenon is much more pronounced at low temperatures. For example, the room-temperature conductivity increases by almost three orders of magnitude between the two extremes of heat treatments. The room-temperature conductivity of the specimen annealed at 60 and 100 °C for 158 and 39 hours, respectively, is on the order of $10^{-4}$ S cm$^{-1}$.

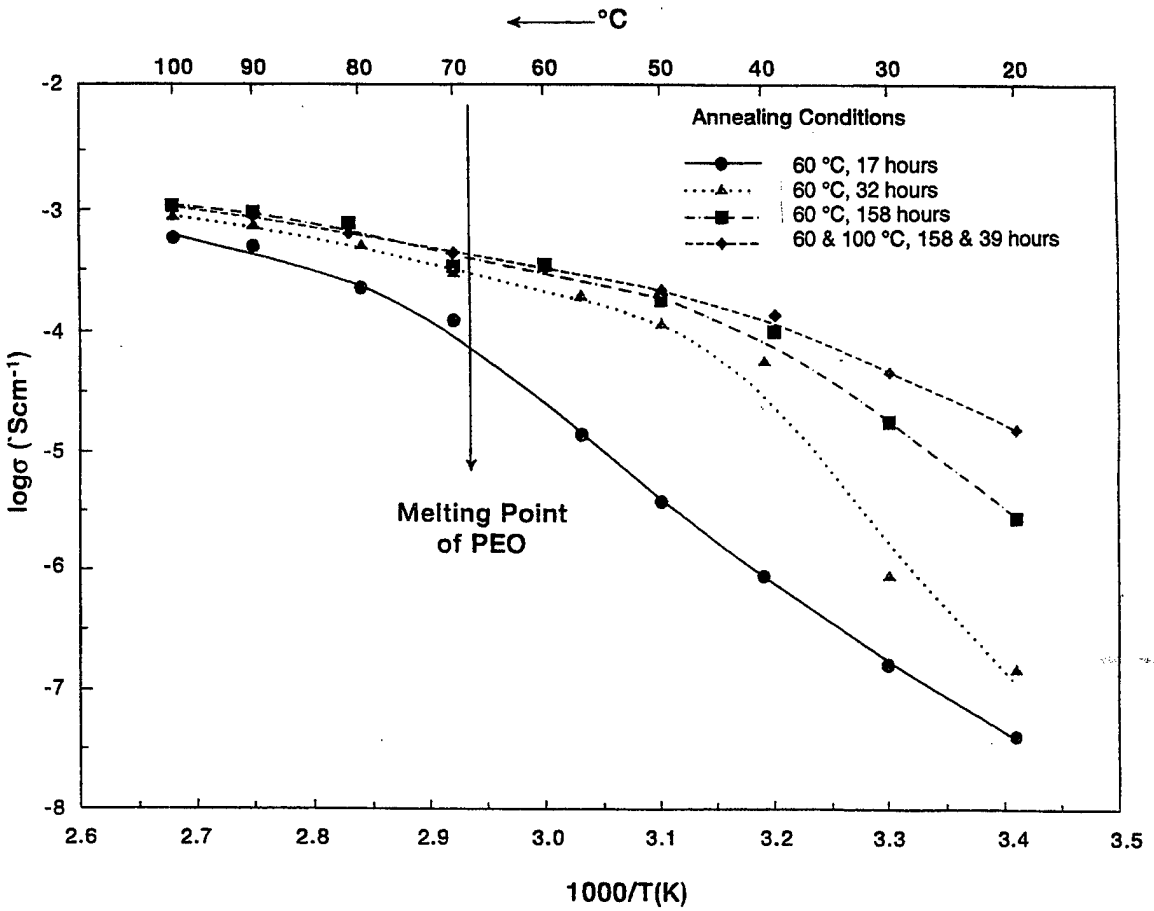


Figure 6. Temperature Dependence of Conductivity of PEO:$LiBF_4$(8:1)-$TiO_2$ (20 wt%, 21 nm) Composite Electrolyte Annealed at 60 and 100 °C

The melting point, $T_m$, of PEO is 68 °C, which is also shown in Figure 6. The specimen annealed at 60 °C for 17 hours shows a transition around 68 °C. Additional annealing at 60 °C (32 hours) improved the conductivity. It should be noted that the annealing temperature, 60 °C, is below the $T_m$, and the thermal state of the specimen is such that it should favor formation of crystalline PEO during the annealing, and using conventional wisdom one should expect a reduction in conductivity. However, the experimental result was just the opposite. A pronounced increase in conductivity was observed after further increasing the annealing temperature to 100 °C. A careful inspection of the conductivity curves in Figure 6 suggests that the transition related to the $T_m$ was depressed to lower temperatures by some 30 °C due to increased heat treatment temperature and time (60 and 100 °C, and 158 and 39 hours, respectively). From 38 to 100 °C, there appears to be a single transport mechanism with low activation energy, 0.31 eV/mol. Below 38 °C the activation energy is increased to a higher value of 1.03 eV/mol.

### 3.2.2 PEO:$LiBF_4$ (8:1)-MgO (10 wt%, 15 nm)

Conductivity data of composite electrolyte films obtained from PEO:$LiBF_4$ (8:1)-MgO (10 wt%) material by the solution cast process are shown in Figure 7. The specimen was heated to and stabilized at 100 °C for 30 minutes, cooled down to 20 °C, and held at that temperature overnight. Subsequently, it was again heated to and stabilized at 100 °C for 30 minutes before the conductivity measurement began. The conductivity data at each temperature was obtained after stabilizing the specimen for 30 minutes. After the temperature reached 20 °C, the specimen was allowed to remain at the temperature overnight.

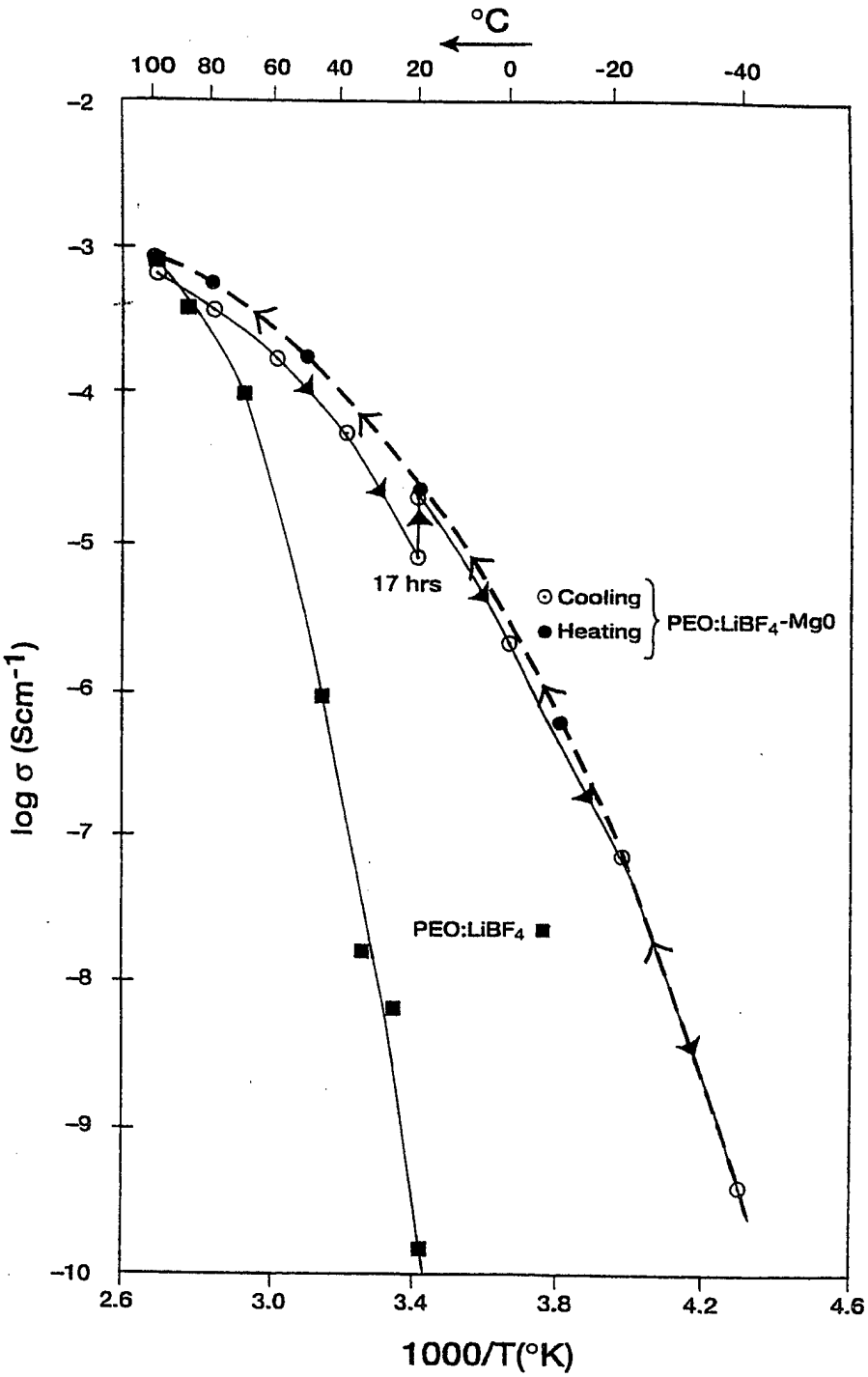


Figure 7. Temperature Dependence of Conductivity of PEO:$LiBF_4$ (8:1)-MgO (10 wt%, 15 nm)

It is noted that log $\sigma$ increased from -5.09 to -4.65. This conductivity enhancement is typical of composite electrolytes. As the temperature was lowered to -40 °C, the conductivity decreased monotonically. Again, the specimen was held overnight at -40 °C before the conductivity was measured during the heating cycle. The conductivities during heating cycles are higher than that of the conductivities during the cooling cycle.

Also shown in Figure 7 is the conductivity data of the PEO:$LiBF_4$ (8:1) polymer complex for comparison purposes. The conductivity of the complex drops precipitously below 60 °C, and at 20 °C this specimen has about four orders of magnitude lower conductivity than that of the composite electrolyte. The comparison clearly points out the role of MgO which retards and eliminates PEO crystallization, thereby imparting beneficial effect on conductivity.

### 3.2.3 PEO:$LiBF_4$ (8:1)-MgO (20 wt%)

After this specimen obtained by the solution cast process was cycled twice between 0 and 100 °C with a cumulative hold time of 18 hours and 106 hours at 100 and 20 °C, respectively, conductivity data were obtained. The data are shown by the curve marked Heating Scan in Figure 8. The conductivity measurement was initiated at 0 °C, data were collected at 20 °C intervals after equilibrating the specimen for 30 minutes at the measurement temperature, and finally the measurement was terminated at 100 °C. The temperature dependence data suggest an absence of crystalline PEO and conductivity values range from $10^{-5.4}$ to $10^{-3.2}$ S $cm^{-1}$ between 0 to 100 °C. After the specimen was held overnight at 100 °C, the conductivity at the temperature decreased from $10^{-3.2}$ to $10^{-3.35}$ S $cm^{-1}$. During the cooling scan to 20 °C, the conductivities remained lower than those of the heating scan. The difference between the heating and cooling scan conductivity values widened as the temperature was lowered.

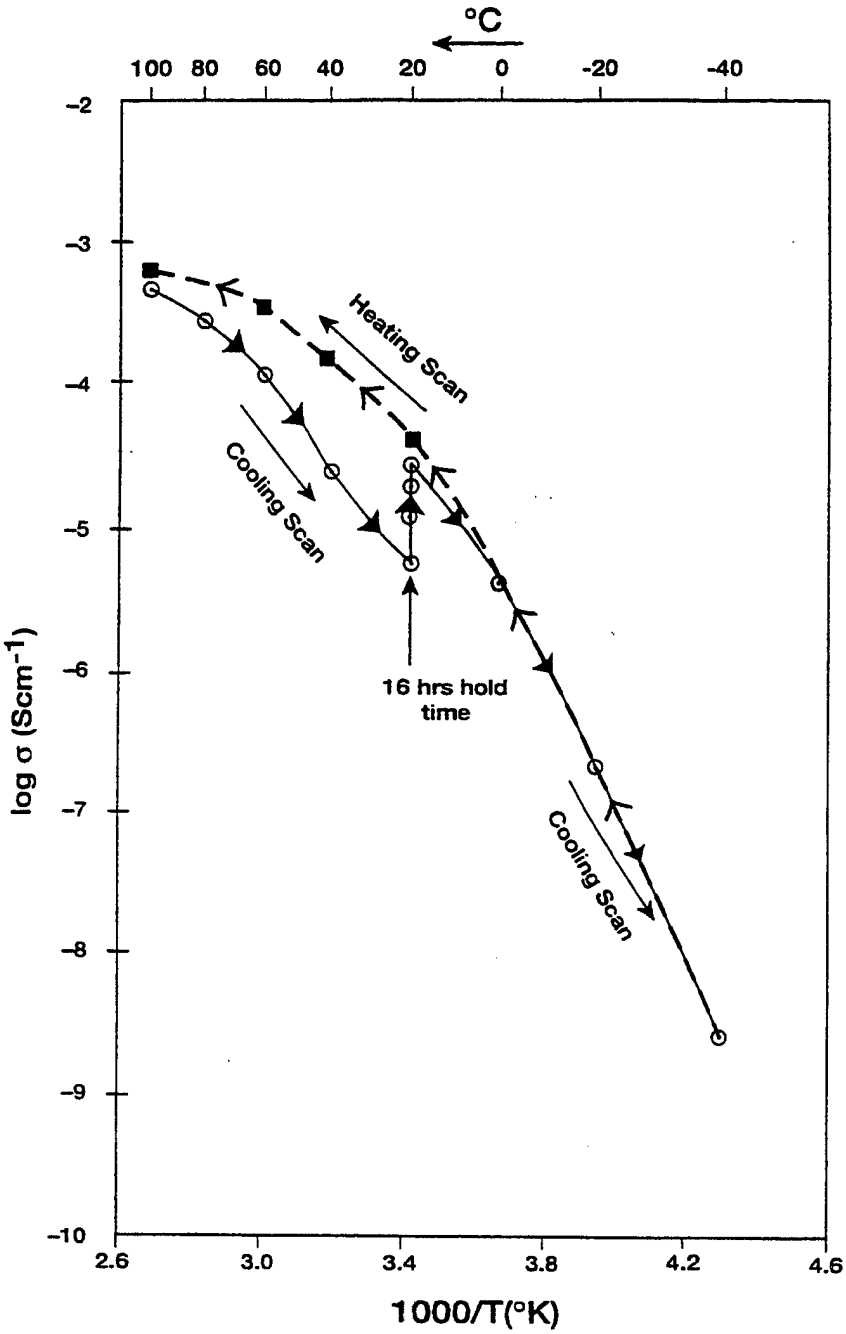


Figure 8. Temperature Dependence of Conductivity of PEO:$LiBF_4$(8:1)-MgO (20 wt%, 15 nm) During Heating and Cooling Scans

At 20 °C, the specimen was allowed to equilibrate overnight. During a span of 16 hours, the conductivity increased from $10^{-5.25}$ to $10^{-4.55}$ S $cm^{-1}$. The time dependence of conductivity enhancement is attributed to polymer chain-ceramic particle interaction and reorientation. This process differs from the polymer crystallization process in which the conductivity generally decreases. With further reduction in temperature, as expected, the conductivity decreased and approached a value of $10^{-8.6}$ S $cm^{-1}$ at -40 °C. The degree of conductivity enhancement during isothermal stabilization at 20 °C is larger as compared to the specimen containing 10 percent MgO (Figure 7). It appears that conductivity enhancement/relaxation is related to the weight fraction of the ceramic phase.

### 3.2.4 PEO:$LiBF_4$ (8:1)-MgO (30 wt%)

The conductivity data of the solution cast PEO:$LiBF_4$ (8:1)-MgO (30 wt%) specimen heat treated under three different parameters are shown in Figure 9. In general, the conductivity decreased with increasing heat treatment temperature and time. A major change in the slope of conductivity plots at 60 °C signifies melting or freezing of the polymer phase. This characteristic was absent in the 10 and 20 percent MgO material (Figures 7 and 8). This leads one to believe that the deterioration in the specimen performance may be linked to the segregation of MgO particles. Furthermore, in specimens containing 30 wt% $TiO_2$ particles [12], it was observed that conductivity generally improved with increasing heat treatment time and temperature. The dielectric constants of MgO and $TiO_2$ are 9.65 and 130, respectively, and it is plausible that MgO particles are more susceptible to thermally-induced motion and aggregation. The conductivity relaxation at 20 °C is also shown in Figure 9 for the specimen heat treated at 40 and 60 °C for 64 and 16 hours, respectively. The conductivity of the specimen subjected to the longest heat treatment time was enhanced by holding the specimen

for 17 hours; however, the conductivity remained lower than prior heat treatments and other specimens.

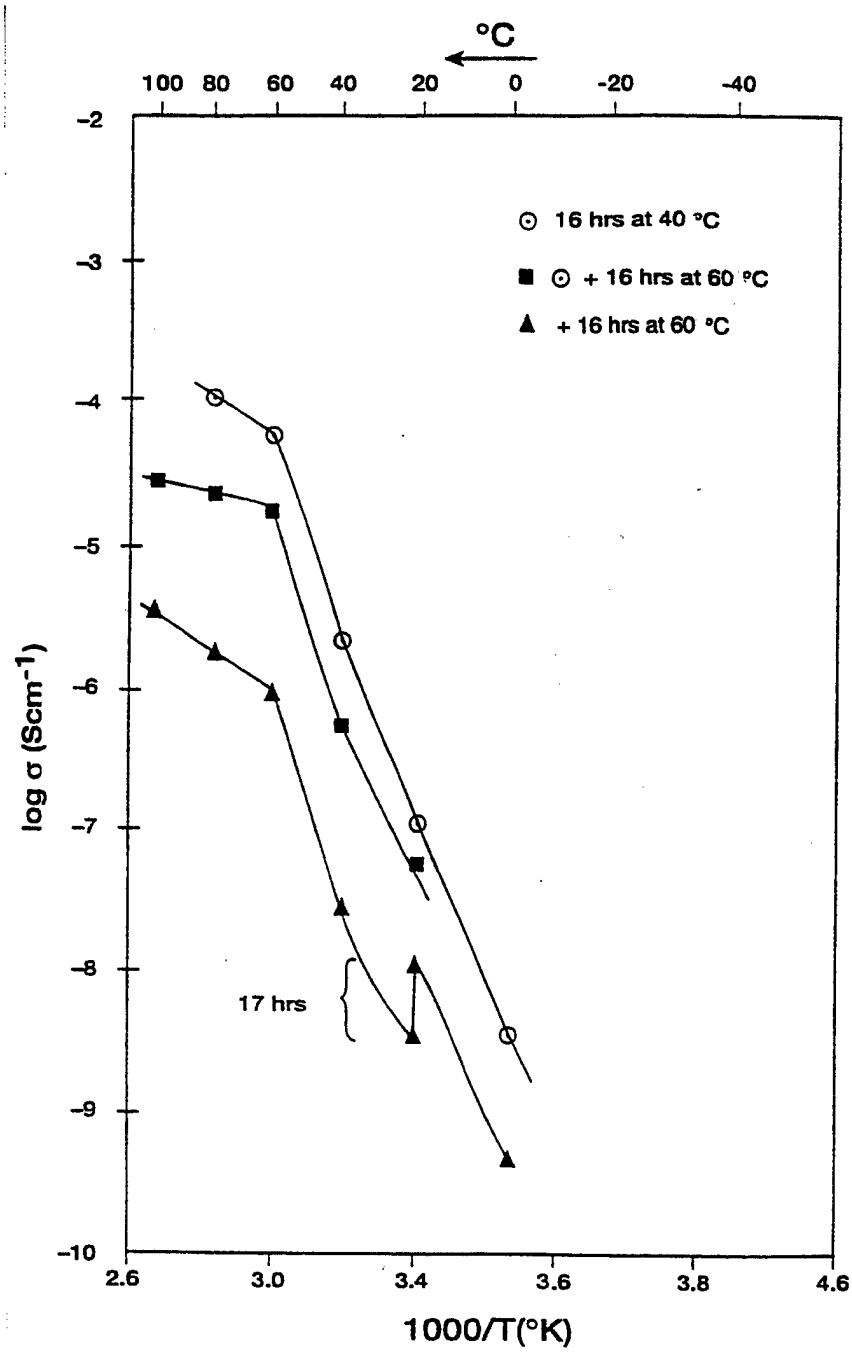


Figure 9. Temperature Dependence of Conductivity of PEO:$LiBF_4$ (8:1)-MgO (30 wt%, 15 nm) Electrolyte Subjected to Three Heat Treatments

### 3.2.5 PEO:$LiBF_4$ (8:1)-$BaTiO_3$ System

Barium titanate ($BaTiO_3$) is a ferroelectric material. Sun, et al. [14] reported that because of spontaneous polarization, $BaTiO_3$ in small amounts enhances the conductivity of composite electrolytes. In view of this information, two composite electrolyte specimens containing $BaTiO_3$ were formulated and characterized.

Figure 10 shows conductivity data of a PEO:$LiBF_4$ (8:1)-$BaTiO_3$ (10 wt%, 70 nm) specimen. The specimen was heat treated at 100 and 60 °C for 2 and 90 hours, respectively. The conductivity values are in fact lower than similar specimens containing MgO, as shown in Figure 7. The data connected by a broken line were obtained during a cooling scan. When the specimen was held at 40 and -20 °C, the conductivity increased – a phenomenon observed in the composite electrolytes. Figure 10 clearly demonstrates that there is no benefit in using $BaTiO_3$ as compared to MgO.

It was suspected that perhaps 10 percent $BaTiO_3$ is too high a concentration to allow spontaneous polarization. Thus, another specimen was formulated with a mixture of MgO (18.5 wt%) and $BaTiO_3$ (1.5 wt%). The temperature dependence of conductivity of the specimen during the heating scan is shown in Figure 11. The conductivity data of this specimen in comparison to the data of 10 wt% MgO (Figure 8) reveals that again there is no benefit derived from the use of $BaTiO_3$. In fact, the conductivity of the specimen containing $BaTiO_3$ is lower than that of the specimen containing only MgO. The relaxation effect was purposely excluded in Figure 11.

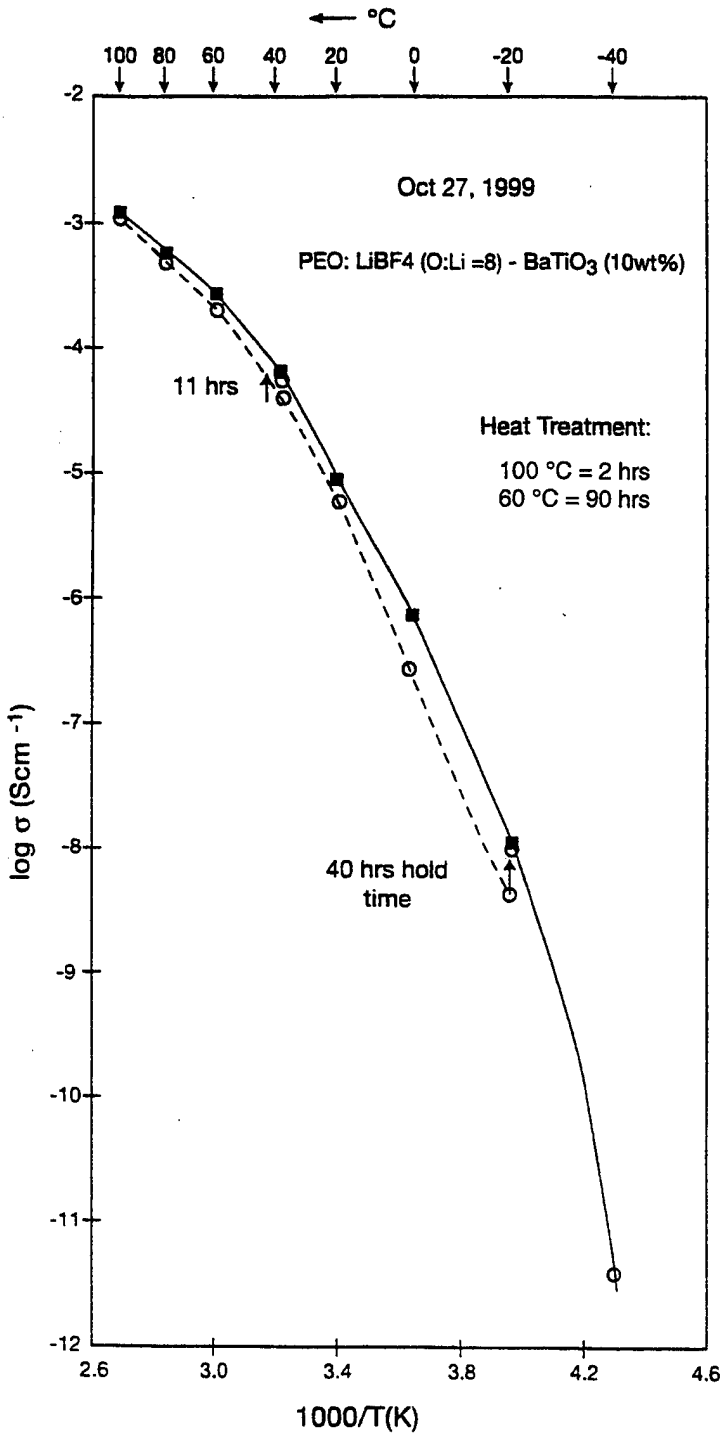


Figure 10. Temperature Dependence of Conductivity of PEO:$LiBF_4$(8:1)-$BaTiO_3$ (10 wt%) Annealed at 100 and 60 °C for 2 and 90 Hours, Respectively

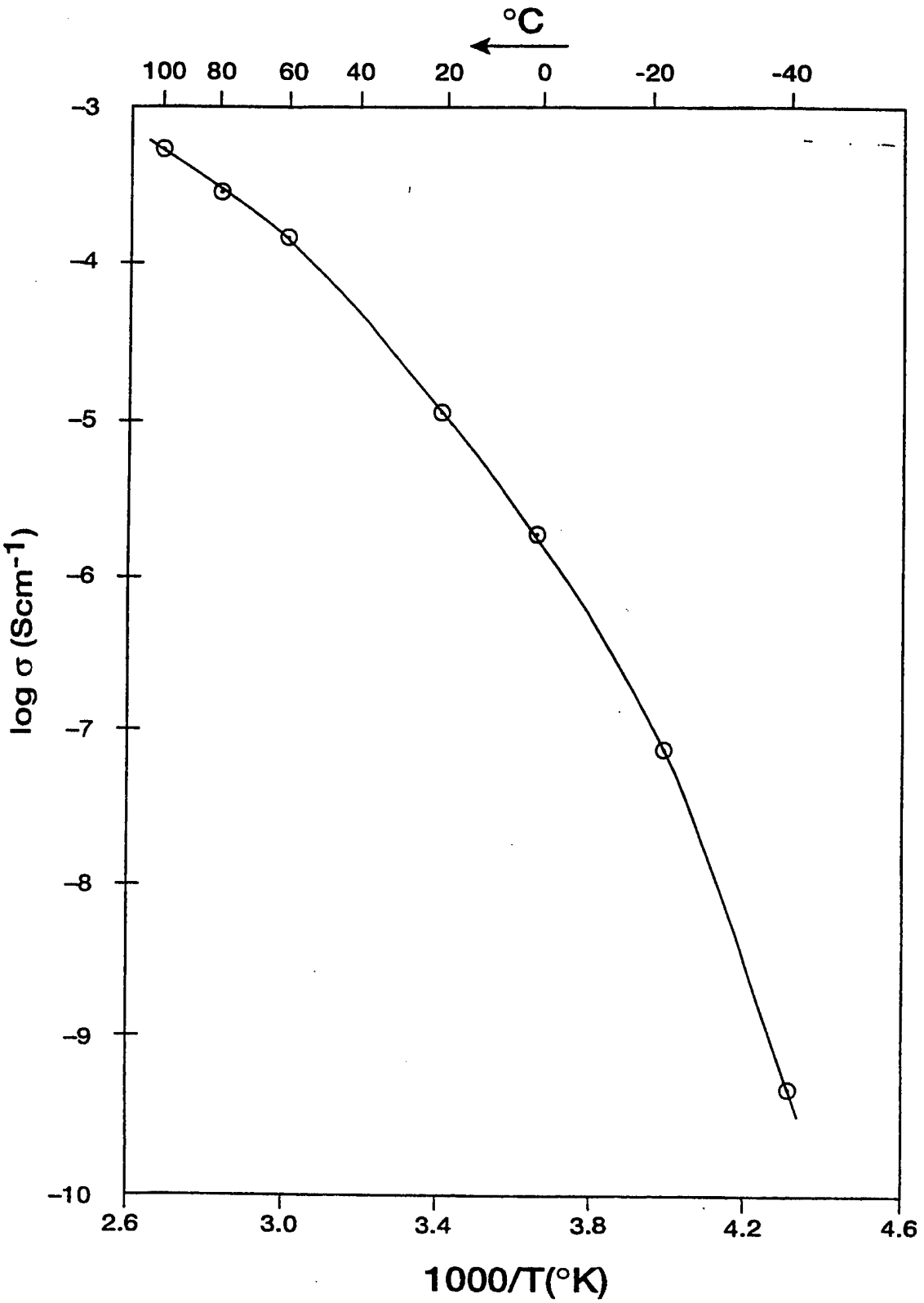


Figure 11. Temperature Dependence of Conductivity of PEO:$LiBF_4$ (8:1)-MgO:$BaTiO_3$ (18.5 wt% and 1.5 wt%, Respectively).

### 3.2.6 Relative Comparison of Composite Electrolytes

Table 1 presents attributes and characteristics of a diverse range of the composite electrolytes investigated in this program. Table 1 illustrates the complexity of composite electrolyte materials. There are a number of variables; some of those identified in the table affect conductivity and temperature dependence of conductivity. The important variables are believed to be the characteristics of ceramic oxide particle size, weight fraction, PEO:$LiBF_4$ ratio, annealing parameters, and degree of polymer crystallinity. Very high dielectric constant ceramics such as $TiO_2$ and $BaTiO_3$ appear to have little influence on conductivity. The PEO:$LiBF_4$ ratio of 8:1 provides the highest conductivity values. All the composite electrolytes exhibit conductivity relaxation which increases, reaches some optimum value, and then decreases with the weight fraction of the ceramic phase. The highest conductivity was obtained in the material that contained 10 to 20 wt% ceramic phase and a polymer complex with a PEO:$LiBF_4$ ratio of 8:1.

## 3.3 CONDUCTIVITY RELAXATION

From the preceding data on the temperature dependence of conductivity, it is quite apparent that the conductivity of a mixture containing PEO, a PEO:$LiBF_4$ complex, and a ceramic phase is sensitive to heating or cooling rates and heat treatment temperatures. The structure may either be retained in a totally amorphous state, or as a mixture of crystalline and amorphous states. This nonequilibrium nature of the structure below the $T_m$ is expected to have a major influence on the lithium ion conductivity. The structure and lithium ion conductivity relationship can be quantified by monitoring the relaxation of conductivity at a given temperature.

Table 1. Composition of Materials: Effect of Variables

| Ceramic Powder | Density ($gm/cm^3$) | Mean Particle Size | Dielectric Constant ($\kappa$) | PEO Mol. Wt. (g/mol) | PEO:$LiBF_4$ Ratio | Wt.% of Ceramic Powder | Range of $\sigma$ ($S\ cm^{-1}$) -20 to 100°C | $\sigma$ Relaxation | $\sigma$ vs/ Temp. | Comments |
|---|---|---|---|---|---|---|---|---|---|---|
| BN | 2.20 | <44 µm | 7.1 | 2,000,000 | 8:1 | 20 | $10^{-9.28}$-$10^{-3.08}$ | Not investigated | Distinct knee between 20 and 60° C. | Color - White |
| $ZrO_2$ | 5.83 | 31 nm | 12.50 | 2,000,000 | 8:1 | 20 | $10^{-8.39}$-$10^{-2.85}$ | Yes | Average $\sigma$ decrease from 100 to -20 °C gradual | Color - White |
| $TiO_2$ | 4.26 (rutile) | 25 nm | $\kappa_{11}=\kappa_{22}=170$ $\kappa_{33}=86$ | 2,000,000 | 8:1 | 20 | $10^{-8.95}$-$10^{-2.58}$ | Yes | Average $\sigma$ decrease from 100 to -20 °C gradual | Double semicircle @ 20 °C Color - Beige |
| MgO | 3.58 | 5-7 µm | 9.65 | 2,000,000 | 8:1 | 10 | $10^{-9.46}$-$10^{-3.00}$ | Yes | Distinct knee between 20 and 60 °C. Low temp. $\sigma$ not good compared to sample with nanosize powder. | Ceramic powder calcined @ 500 °C Color - Yellowish Brown |
| MgO | 3.58 | 9 nm | 9.65 | 200,000 | 8:1 | 20 | $10^{-10.14}$-$10^{-3.03}$ | Yes | Distinct knee between 20 and 60 °C. Better low temp. $\sigma$ good compared to sample with micron size powder. | Color - Dark Brown |
| MgO | 3.58 | 9 nm | 9.65 | 8,000,000 | 8:1 | 20 | $10^{-8.72}$-$10^{-2.89}$ | Yes | Distinct knee between 20 and 60 °C. | Two films (3.5 mil) sandwiched together Color - Dark Brown |
| MgO | 3.58 | 9 nm | 9.65 | 8,000,000 | 8:1 | 20 | $10^{-8.70}$-$10^{-3.11}$ | Yes | Distinct knee between 20 and 60 °C. | Single film 3.25 mil; Color - Dark Brown |
| $Al_2O_3$ | 3.95 | 24 nm | 8.6-10.6 | 2,000,000 | 8:1 | 20 | $10^{-8.56}$-$10^{-2.58}$ | Yes | - | Annealed 2 hrs @ 175 °C after melt mix. Rubbery, Color - Dark Brown |
| $Al_2O_3$ | 3.95 | 24 nm | 8.6-10.6 | 2,000,000 | PEO:$LiBF_4$:$LiPF_6$ 8 : 0.5 : 0.5 | 20 | $10^{-7.38}$-$10^{-2.81}$ | Yes | - | Annealed 1 hr @ 100 °C after melt mix. Waxy, Color - Black |
| $BaTiO_3$ | 6.02 (T) | 40-100 nm | $\kappa_{11}=3600$ $\kappa_{33}=150$ | 2,000,000 | 8:1 | 10 | $10^{-8.1}$-$10^{-3}$ | Yes | - | Conductivity improved after aging at 100 and 60 °C. |

A system in a nonequilibrium state proceeds toward an equilibrium state at a unique rate determined by thermodynamic parameters. Such a system is under internal stress, and the transformation occurs to relieve the stress. The result of this transformation is a change in the physical properties (in the present situation, the conductivity) of the material which occurs through a molecular rearrangement. In this case, the transformation may occur either by nucleation and crystallization of PEO spherulites or polymer-ceramic dipole interaction. The transformation relieves the internal stresses at points known as relaxation sites. The kinetics of the relaxation largely depends upon the characteristics of the relaxation site. A system may also possess more than one kind of relaxation site. Associated with the various relaxation sites are characteristic relaxation times.

The conductivity relaxation of composite electrolytes at a given temperature may be expressed by equation (2):

$$\sigma'(t) = \sigma(\infty) \pm \sum_{i=o}^{n} \sigma_i e^{-\nu_i t} \qquad (2)$$

where $\sigma'(t)$ = conductivity at time t

$\sigma(\infty)$ = equilibrium conductivity

$\sigma_i$ = relaxation amplitude

$\nu_i$ = relaxation frequency ($1/\tau_i$)

$\tau_i$ = relaxation time.

If it can be assumed that there is only one kind of relaxation site or mechanism at the measurement temperature, equation (2) can be reduced to:

$$\sigma(t) = \sigma'(t) - \sigma(\infty) = \sigma_o e^{-\nu_o t}. \qquad (3)$$

Conductivity relaxation of a specimen, PEO:$LiBF_4$–$ZrO_2$ (30 wt%) with an [O]:[Li] ratio of 12.64:1, is shown in Figure 12. This specimen was held at 150 °C for 6 hours, brought down to 0 °C, and held at this temperature for 6 hours, and then the temperature was raised to 20 °C before the conductivity measurement began. It is noted that the conductivity increased by almost an order of magnitude in a period of 13 hours. The relaxation time, $\tau$, for the measurement was determined to be 11 hours. This relaxation is attributed to the polymer-ceramic dipole interaction. The temperature of this specimen was subsequently raised to 28 °C, and the conductivity was monitored for 335 hours. The conductivity evolution is shown in Figure 13. Although the temperature was increased from 20 to 28 °C, the conductivity dropped and continued its decline until the experiment was terminated. The relaxation time for this process leading to the reduction in conductivity is 400 hours, which is related to the nucleation and crystallization of PEO.

The relaxation data in Figures 12 and 13 demonstrate that the conductivity of the composite electrolytes below the $T_m$ are sensitive to thermal histories. Conductivity variations of two orders of magnitude at a given temperature (<68 °C) can be expected and attributed to the thermal history. The observed relaxation is one characteristic of a metastable, supercooled liquid structure. The crystalline ceramic particles such as $TiO_2$ and $ZrO_2$ slow down the relaxation and increase the relaxation time to the extent that they can be measured and analyzed.

Figure 14 schematically shows the conductivity-temperature relationship of a typical polymer-ceramic composite electrolyte. The polymer liquid can be supercooled below the crystallization temperature, $T_c$, down to the glass transition temperature, $T_g$. In such a situation, the temperature dependence of conductivity should exhibit the Arrhenius relationship. Any deviation, such as crystallization at temperature ($T_c' < T_c$) would lead to a deviation from the

idealized behavior of the supercooled liquid, and result in a nonlinearity in log σ versus 1000/T plots. Another deviation of greater magnitude would occur as the glass transition temperature ($T_g$) is approached, where the structural relaxation diminishes by many orders of magnitude. For these polymer-ceramic electrolytes the experimental data are not available near and below the $T_g$.

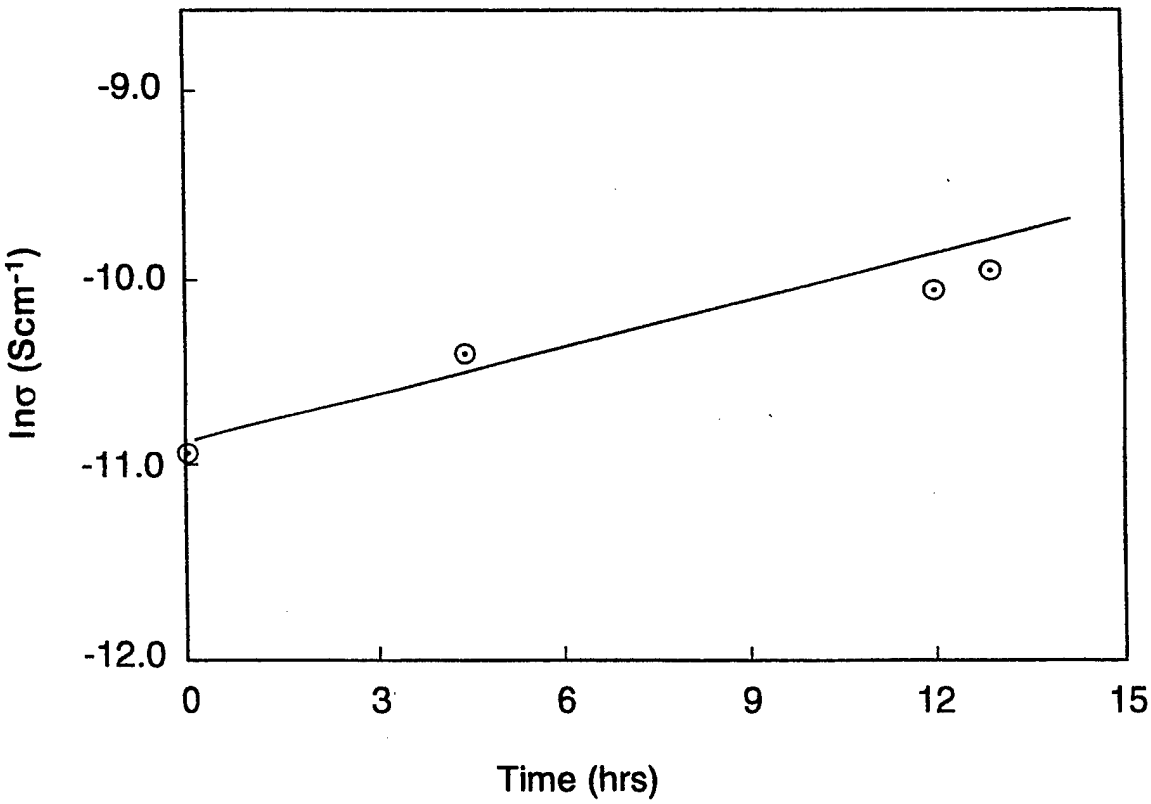


Figure 12. Conductivity Relaxation of the PEO:$LiBF_4$-$ZrO_2$ (30 wt%) at 20 °C, [O]:[Li] = 12.64:1
The Specimen was Heat Treated at 150 °C for 6 Hours, Rapidly Cooled Down to and Held at 0 °C for 6 Hours, and Subsequently Heated Up to 20 °C Before Conductivity Measurement

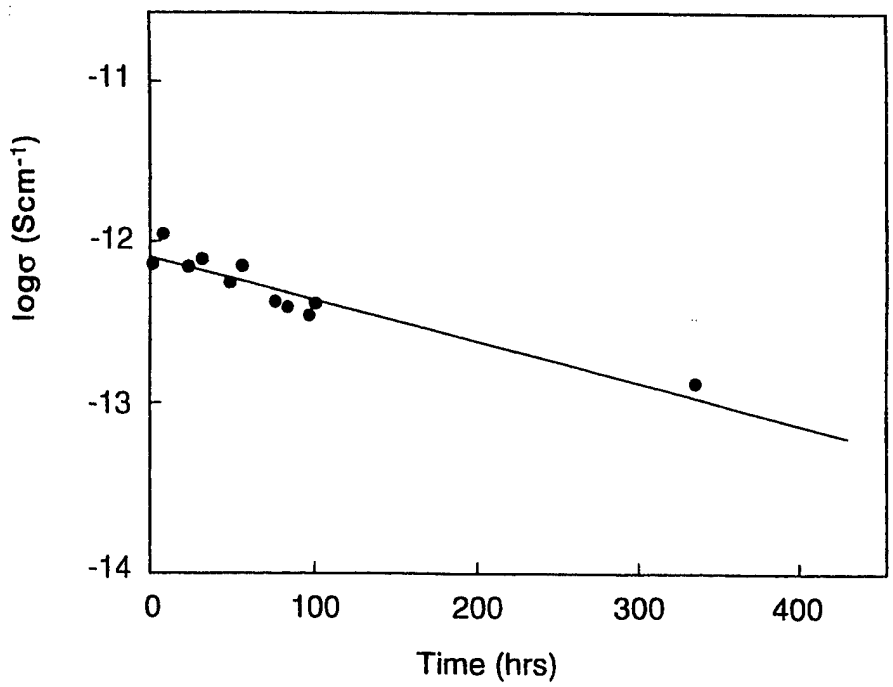


Figure 13. Conductivity Relaxation at 28 °C in PEO:$LiBF_4$ (12.64:1)-$ZrO_2$ (30 wt%)

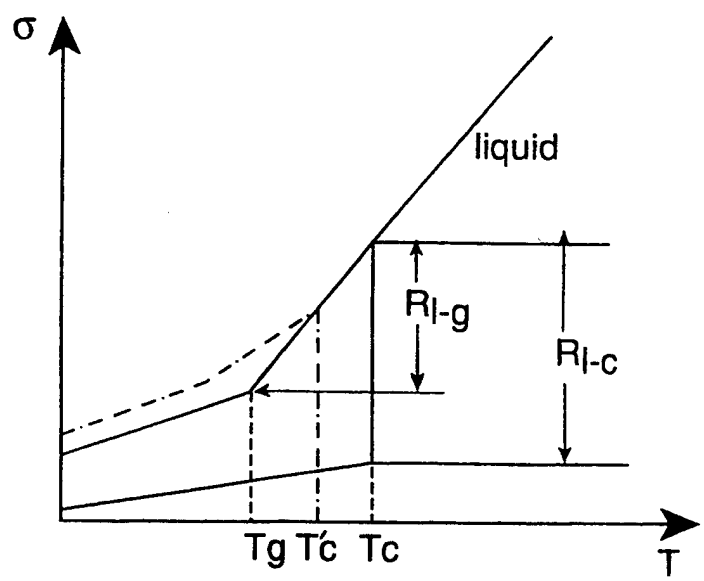


Figure 14. Schematic of Conductivity Relaxation Regions in Polymer-Ceramic Composite Electrolytes

In the temperature range between $T_c$ and $T_g$, conductivity relaxation is expected to be significant and measurable. At or near the $T_g$, the relaxation time is of the order of hours and days. As one approaches $T_c$ from the $T_g$, the relaxation time becomes smaller, to the extent that it may be less than the time of experimental observation. Since the relaxation is characteristic of and associated with a polymeric liquid-like structure and not the crystalline ceramics, it is conceivable that with an increased volume fraction of the ceramic phase, the relaxation time can be increased to such an extent that the structure becomes stable for all practical purposes.

## 3.4 EFFECT OF PARTICLE SIZE

### 3.4.1 Conductivity as Influenced by the Size of Ceramic Additive

#### 3.4.1.1 PEO:$LiBF_4$ (8:1)-MgO (10 wt%) Materials

Temperature dependence of conductivity of the PEO:$LiBF_4$ complex and PEO:$LiBF_4$ (8:1)-MgO (10 wt%) materials containing micro- and nano-size MgO are shown in Figure 15. All these specimens were cycled three times between 20 and 100 °C while holding them for a total cumulative time of 1 hour at 100 °C and 40 hours at 20 °C. The thermalization process was determined to be adequate to stabilize and optimize conductivity values. Furthermore, at each temperature the specimen was held for 30 minutes before an impedance measurement was conducted.

The lowest conductivity values are associated with the PEO:$LiBF_4$ (8:1) complex. Near the melting point of PEO, 68 °C, a precipitous drop in conductivity begins and at around ambient temperature the conductivity drops to $10^{-9}$ S cm$^{-1}$. The specimen containing micro-size ($\simeq$ 5 μm) MgO exhibits much improved conductivity as compared to the PEO:$LiBF_4$ complex.

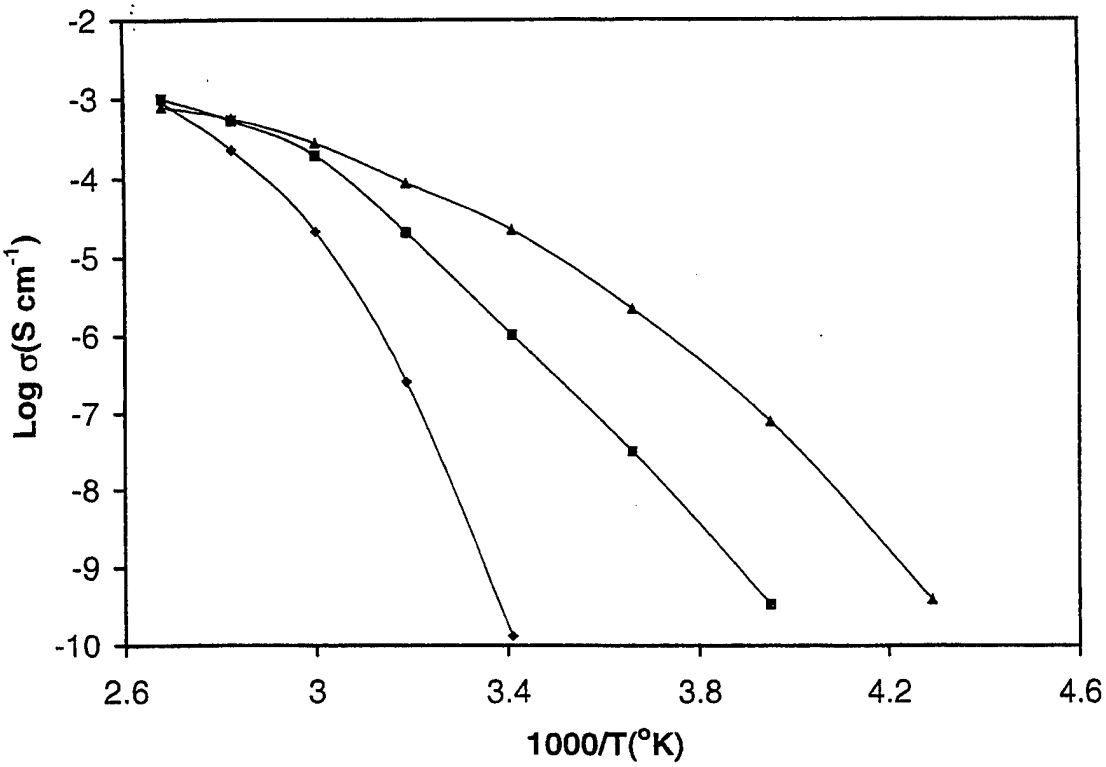


Figure 15. Temperature Dependence of Conductivity of PEO:$LiBF_4$(8:1) Electrolyte Doped with Nano- and Micro-size MgO
PEO:$LiBF_4$ (8:1) Complex - ◆; PEO:$LiBF_4$ (8:1)-MgO (10 wt%) Micro-size - ■, and PEO:$LiBF_4$ (8:1)-MgO (10 wt%) Nano-size - ▲

Around ambient temperature, the conductivity is improved by approximately three orders of magnitude by incorporating micro-size MgO in the polymer complex. This conductivity enhancement is attributed to a large reduction in the crystalline component of the polymer phase. There is a possibility of a residual structural order resembling crystallinity in this composite material, as the entire conductivity curve appears to be composed of two linear segments intersecting at the melting temperature of PEO. The highest conductivity values are associated with the specimen containing nano-size MgO. The conductivity of this specimen is about four orders of magnitude higher than the PEO:$LiBF_4$ complex around the ambient temperature. Furthermore, the temperature dependence of conductivity diminished as the MgO particle was reduced from micro- to nano-size. At 100 °C, all three specimens possess similar conductivity values, whereas the curves diverge as the temperature is lowered to -40 °C. It should also be noted that major benefits in conductivity enhancement are realized at lower temperatures by the incorporation of MgO. It has also been reported [15] that increasing the concentration of nano-size MgO from 10 to 20 wt% makes insignificant difference in conductivity values.

#### 3.4.1.2 PEO:$LiBF_4$ (8:1)-$BaTiO_3$ (20 wt%) Materials

The temperature dependence of conductivity of the PEO:$LiBF_4$ complex and specimens containing micro- and nano-size $BaTiO_3$ are shown in Figure 16. These specimens also exhibit behavior similar to the MgO containing electrolytes (Figure 15). The low-temperature conductivities are greatly improved by the incorporation of $BaTiO_3$. The nano- and micro-size $BaTiO_3$ specimens, however, exhibit a crossover around 50 °C. The nano-size specimen possesses lower conductivity above 50 °C, but higher conductivity below 50 °C as compared to the micro-size $BaTiO_3$ specimen. This kind of trend was also

noted for MgO (Figure 15), but to a much lower degree. The ambient temperature conductivities of the $BaTiO_3$-containing specimens are in the $10^{-4}$ to $10^{-5}$ $Scm^{-1}$ range.

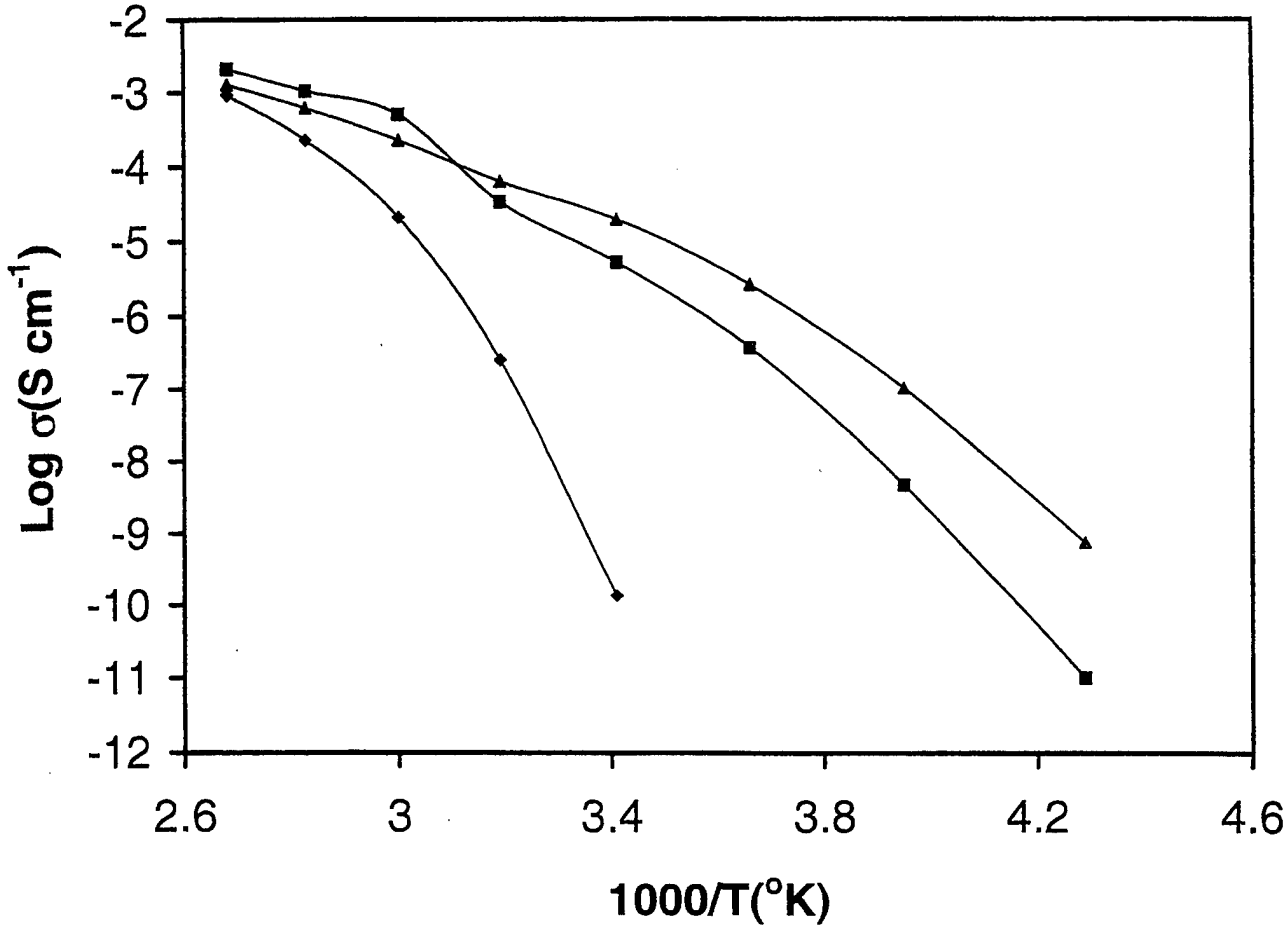


Figure 16. Temperature Dependence of Conductivity of PEO:$LiBF_4$ (8:1) Electrolyte Doped with Nano- and Micro-size $BaTiO_3$
PEO:$LiBF_4$(8:1)-$BaTiO_3$ Complex- ◆; PEO:$LiBF_4$(8:1)-$BaTiO_3$ (20 wt%) Micro-size - ■; and PEO:$LiBF_4$(8:1)- $BaTiO_3$ (20 wt%) Nano-size - ▲

### 3.4.2 Physical Properties of MgO and $BaTiO_3$ Powders

Table 2 presents the physical properties of MgO and $BaTiO_3$ materials. $BaTiO_3$ is an important ferroelectric material and its dielectric constant in the tetragonal phase (ferroelectric state) is much higher and anisotropic. The dielectric constant of $BaTiO_3$ is also known to be particle-size-dependent [16]. The $BaTiO_3$ materials used in this investigation exhibited an endothermic peak around 120 °C during the differential scanning calorimetry measurements, suggesting that they were in the ferroelectric, tetragonal phase, and the dielectric constant of the material as presented in Table 2 is believed to reflect their characteristics.

Table 2. Physical Properties of MgO and $BaTiO_3$

| Ceramic Oxide | Melting Temperature (°C) | Density ($g/cm^3$) | Dielectric Constant ($\kappa$) | Mean Particle Sizes | Masses of a Particle (gm) |
|---|---|---|---|---|---|
| MgO | 2852 | 3.58 | 9.65 | 5 μm, 20 nm | $2.34 \times 10^{-10}$, $1.5 \times 10^{-17}$ |
| $BaTiO_3$ | - | 6.02 (tetragonal) | $\kappa_{11} = 3{,}600$ $\kappa_{33} = 150$ | 1 μm, 70 nm | $9.45 \times 10^{-12}$, $8.65 \times 10^{-15}$ |

The two ceramic materials, MgO and $BaTiO_3$, in effect represent upper and lower limits of dielectric constants of available ceramic materials. The last column of Table 2 shows masses corresponding to the two particle sizes used for each material. For MgO and $BaTiO_3$, the masses corresponding to each particle size differ by approximately seven and three orders of magnitude, respectively. In spite of such a large difference in physical properties of MgO and $BaTiO_3$, they exhibit similar effects on conductivity.

### 3.4.3 Crystalline Characteristics of the Polymer Phase

It is evident from Figures 15 and 16 that a ceramic phase in either micro- or nano-size form enhances conductivity. It should also be appreciated that the PEO:$LiBF_4$ (8:1) complex and its composites with ceramic phases possess an inherent tendency to crystallize. The amorphous-to-crystalline transition is sluggish, nonetheless it is present and must be dealt with and accounted for. The DSC scans of a PEO:$LiBF_4$ (8:1)-MgO (10 wt%) specimen containing micro-size MgO is shown in Figure 17. The specimen has been cycled six times as indicated by a run number between 25 and 200 °C at the heating and cooling rates of 10°C per minute. The cumulative hold times at 25 °C for each of the runs are shown in Figure 17. In six cycles with a total of 162 hours of hold time at 25 °C, the crystalline component was eliminated. Without any hold time at 25 °C, the crystalline component can be eliminated in only three cycles with similar heating and cooling rates.

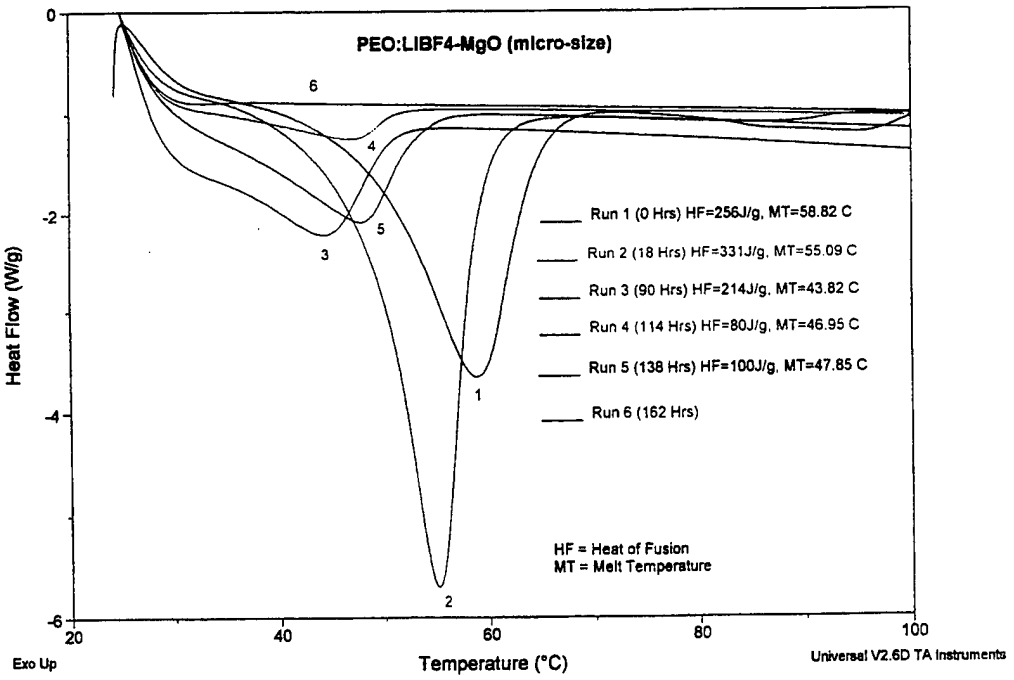


Figure 17. DSC Data of PEO:$LiBF_4$ (8:1)-MgO (10 wt%, Micro-size) Specimen Aged at 25 °C for Various Times

These experiments have led us to believe that an amorphous structure possessing long-term stability can be produced in these composite electrolytes with either a nano- or micro-size ceramic component.

### 3.4.4 The Dominant Variable

In spite of widely different physical characteristics, including density and dielectric constant, both MgO and $BaTiO_3$ additives exhibit similar effects with regard to the particle size, thus it is believed to be a dominant parameter. Reducing the particle size from the micro- to nano-range increases low-temperature conductivities and decreases their temperature dependence, as shown in Figures 15 and 16. The enhancements are pronounced and associated with lower activation energies for the lithium transport.

The average length and mass of a PEO chain are 20 μm and $3x10^{-18}$ gm, respectively. These length and mass values must now be compared with a particle size and mass of the ceramic dopants to develop an insight into possible interactions. Schematically, the proximity and interaction of a polymer chain and a nano-size MgO particle (0.02 μm) are shown in Figure 18. A constant segmental chain motion at ambient temperature, approximately 70 °C above the glass transition temperature, is expected to cause displacement and distribution of MgO particles. Furthermore, the process can be facilitated by thermal treatments and cycling. The displacement and distribution of MgO particles continues until the polymer chain dipole and MgO dipole interaction takes place. The interaction leads to latching of the polymer chain and MgO particle and thus stabilization of the structure. When experimentally monitored, this phenomenon is reflected by an increase in conductivity during isothermal stabilization at low temperatures.

The degree of polymer chain and ceramic particle interaction can be reduced by adding a heavier, fewer, and lower weight or volume percent of MgO. For example, if the weight percent of MgO is maintained constant and the particle size is reduced from 5 μm to 20 nm, over 15 million additional polymer-ceramic interaction sites are created and conductivity enhancements occur. Table 2 also shows that reducing particle size from 5 μm to 20 nm reduces the mass of a particle by seven orders of magnitude. These lighter MgO particles become far more receptive to the segmental chain motion of the polymer, leading to improved polymer chain and MgO particle interaction. Such an interaction is reflected by an enhanced and time dependent conductivity.

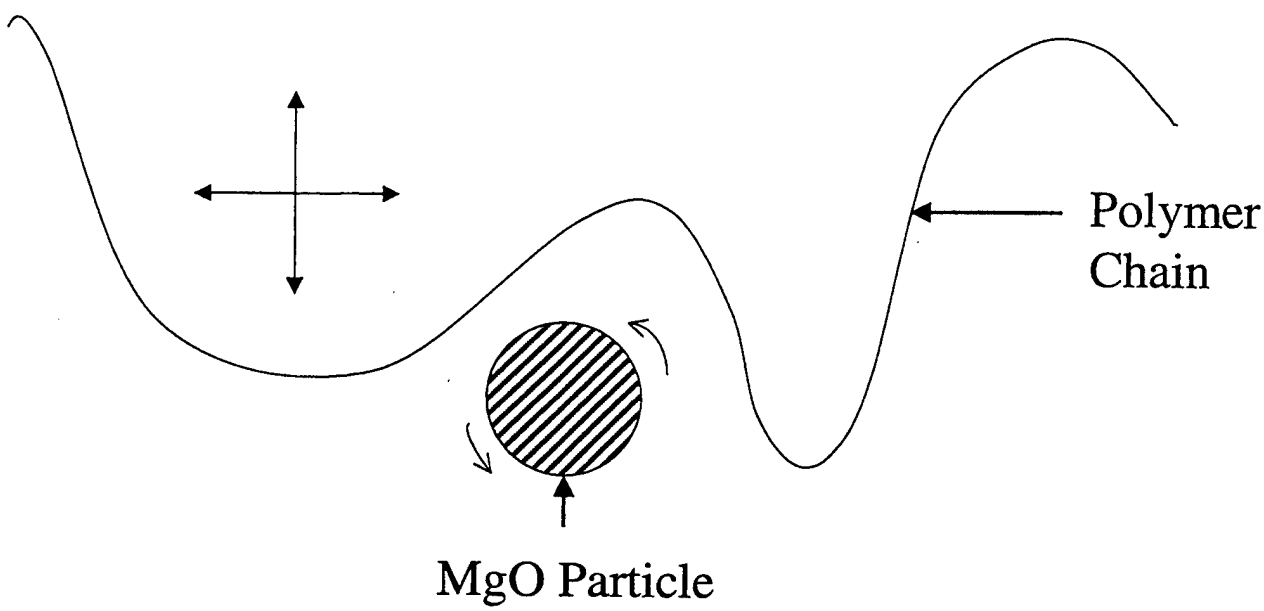


Figure 18. Schematic Representation of a Polymer Chain Segment and MgO Particle Interaction

## 3.5 CRYSTALLINE ⇔ AMORPHOUS TRANSITION

A predominance of the amorphous phase is desirable if one is interested in a material with high conductivity. The fast ionic transport takes place in the amorphous phase in which the conductivity is about two to three orders of magnitude greater as compared to the crystalline phase [10]. It has also been reported that the crystalline ⇔ amorphous transition is sluggish, which leads to the thermal history dependent conductivity [17]. The transition also takes place around ambient temperature and within the operating temperature range of lithium batteries. Since the transition can lead to a conductivity variation up to four orders of magnitude [12], it is critical to understand and characterize the crystalline ⇔ amorphous transition.

The choice of initiators allows synthesis of linear PEO polymers with a wide range of molecular weights (20,000 to 8,000,000). The regularity of polymerized units leads to a high degree of crystallinity; in some cases up to 85 percent. The sluggish nature of the crystalline ⇔ amorphous transition facilitates supercooling and long-term retention of the amorphous structure over a wide temperature range.

The polymer-ceramic composite electrolytes prepared either by solution or melt casting exhibit partial crystallinity of the polymer phase [12, 17]. The crystalline phase can be reduced to an amorphous state by a number of techniques such as crosslinking polymer networks with short chains of ethylene oxide, using doping salts which form low temperature eutectics with a PEO phase, employing organic plasticizers, and incorporating a ceramic component. The last technique provides many advantages over other techniques [7]. This section of the report is primarily based on this technique of converting the crystalline to amorphous phase and its subsequent stabilization.

### 3.5.1 Differential Scanning Calorimetry and Thermogravimetric Analysis Measurements

The DSC scan of a PEO:$LiBF_4$ (8:1)-$Al_2O_3$ (20 wt%, 24 nm) specimen prepared by the melt casting process with an additional thermal treatment at 100 °C for 1 hour is shown in Figure 19. The specimen was subjected to a heating rate of 10 °C $min^{-1}$ from room temperature to 150 °C, and held at this temperature for 1 hour. Subsequently, the specimen was cooled down to room temperature at the rate of 10°C $min^{-1}$. The specimen was then allowed to equilibrate at room temperature for 1 hour before the second heating cycle began at the rate of 10 °C $min^{-1}$. The DSC measurement was terminated after the specimen reached 130 °C. During the first heating cycle, two endothermic peaks located around 61.6 and 91.1 °C were attributed to the melting of PEO and PEO:$LiBF_4$ complex, respectively. During the cooling scan, there was no recrystallization peak which would have been apparent by the appearance of an exothermic peak. After the specimen was stabilized at room temperature for 1 hour and subsequently heated for the second time, a complete disappearance of the crystalline PEO phase was observed.

Table 3 presents important parameters obtained from the DSC measurements conducted on five specimens subjected to different thermal treatments. The parameters are heats of fusion (J $g^{-1}$) as obtained by the area under the peaks and peak locations. The thermal treatment of the film is the only variable of the thermal cycling experiment. As the thermal treatment temperature was increased from 100 to 175 °C, the second endothermic peak corresponding to the melting of PEO:$LiBF_4$ complex was eliminated and the intensity of the first peak decreased while the peak temperature shifted toward a lower temperature. As the thermal treatment time at 175 °C was increased from 1 to 2 hours, the first peak was eliminated. At this point, the specimen primarily consisted of an amorphous phase.

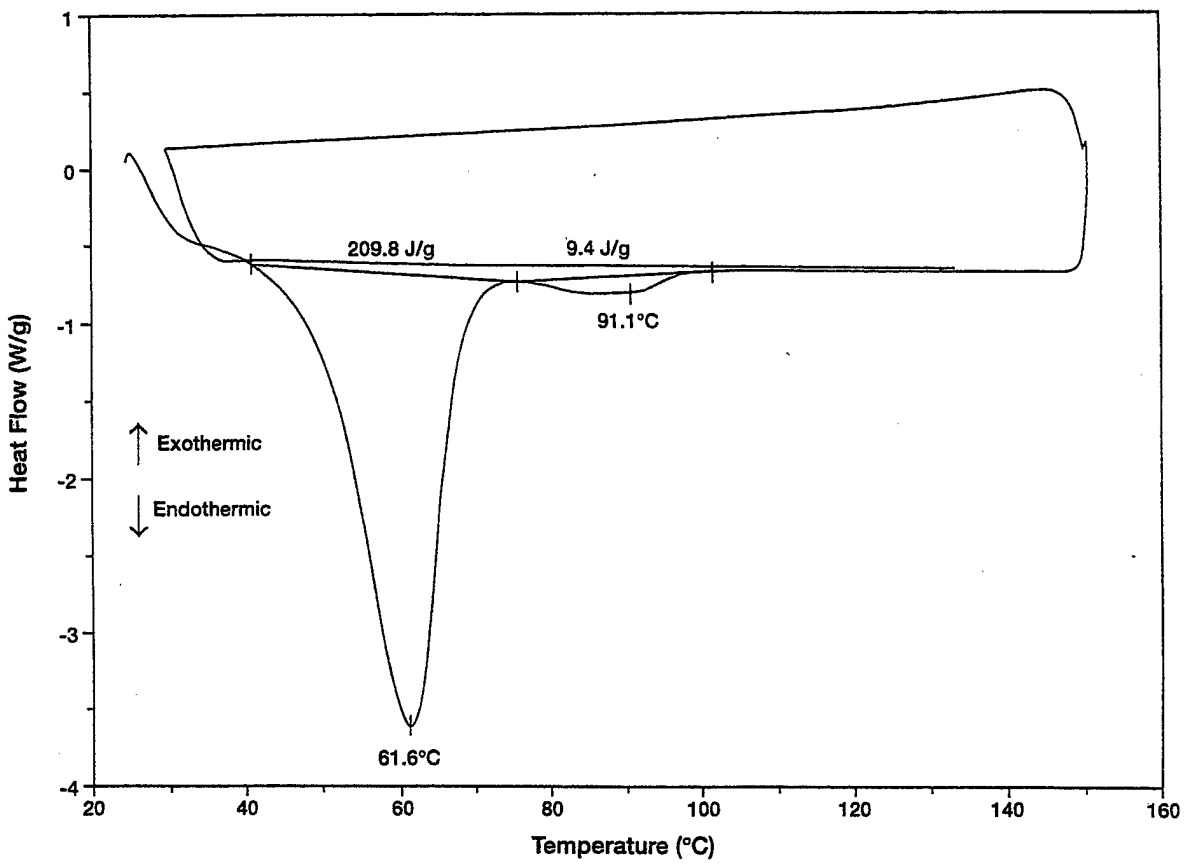


Figure 19. DSC Scans of PEO:$LiBF_4$ (8:1)-MgO (20 wt%, 24 nm) Specimen Subjected to a Thermal Treatment at 100 °C for 1 Hour

Table 3. DSC Parameters as Influenced by Thermal Treatments

| Thermal Treatment | Peak 1 (PEO) | Peak 2 (PEO:$LiBF_4$ Complex) |
|---|---|---|
| 1 hour @ 100 °C | 209 J/g, 62 °C | 4.3 g, 91 °C |
| 1 hour @ 150 °C | 204 J/g, 59 °C | 11 J/g, 90.5 °C |
| 1 hour @ 175 °C | 30 J/g, 49 °C | — |
| 1.5 hours @ 175 °C | 2 J/g, 47 °C | — |
| 2 hours @ 175 °C | — | — |

Figure 20 shows the thermogravimetric analysis (TGA) data of PEO obtained at a heating rate of 10 °C $min^{-1}$. Significant decomposition of PEO began at 200 °C with the decomposition peak located at 378.6 °C. Thus the upper thermal treatment temperature, 175 °C, as shown in Table 3 is well below the decomposition temperature of PEO.

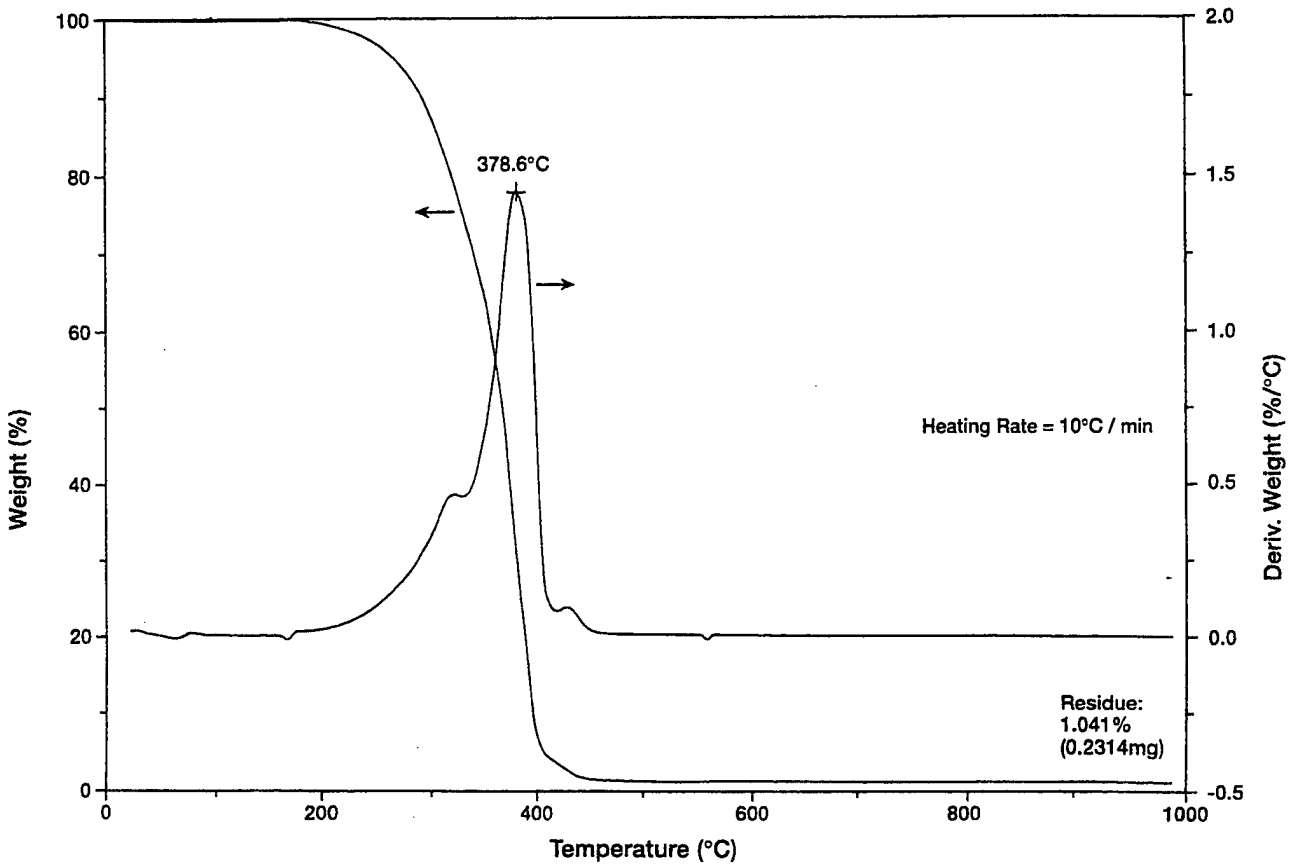


Figure 20. TGA Scan of PEO in the 0 to 1000 °C Range Showing a Decomposition Peak Temperature at 378.6 °C

### 3.5.2 Effect of $Al_2O_3$ Particle Size on Crystalline ⇔ Amorphous Transition

Three different particle sizes, 24 nm, 10 μm, and 100 μm, of $Al_2O_3$ were used in a specimen of PEO:$LiBF_4$ (8:1)-$Al_2O_3$ (20 wt%) composition prepared by the melt casting process. Following the process, these specimens were cycled twice using heating and cooling rates of 10 °C $min^{-1}$ between ambient temperature and 100 °C. The hold times at ambient and 100 °C were 60 and 30 minutes, respectively. The DSC curves corresponding to 24 nm, 10 μm, and 100 μm size particles are shown in Figures 21 through 23, respectively. All three specimens show the presence of crystalline PEO. The thermal cycling reduces crystallinity in these specimens; however, the specimen containing the nano-size (24 nm) $Al_2O_3$ is the most conspicuous with respect to a reduction in crystallinity due to thermal cycling (Figure 21).

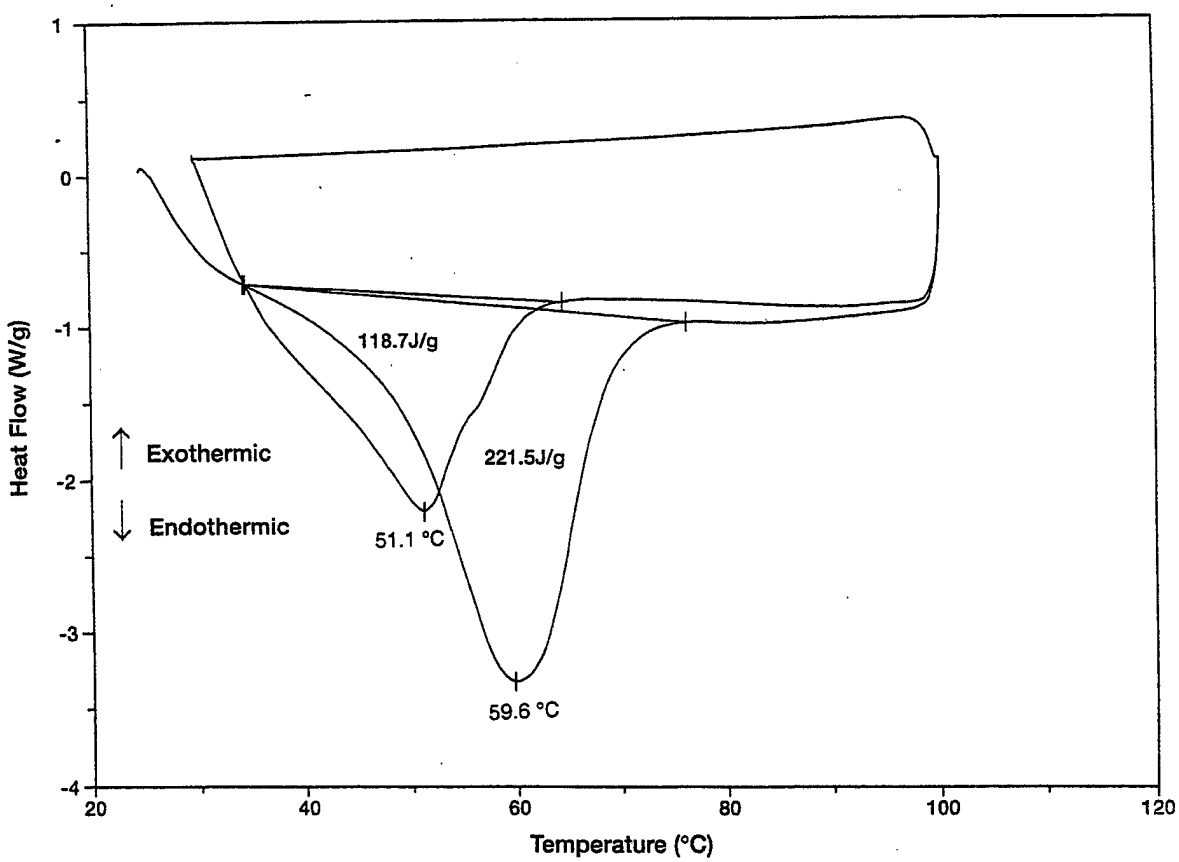


Figure 21. DSC Scans of PEO:$LiBF_4$ (8:1)-$Al_2O_3$ (20 wt%, 24 nm) Specimen

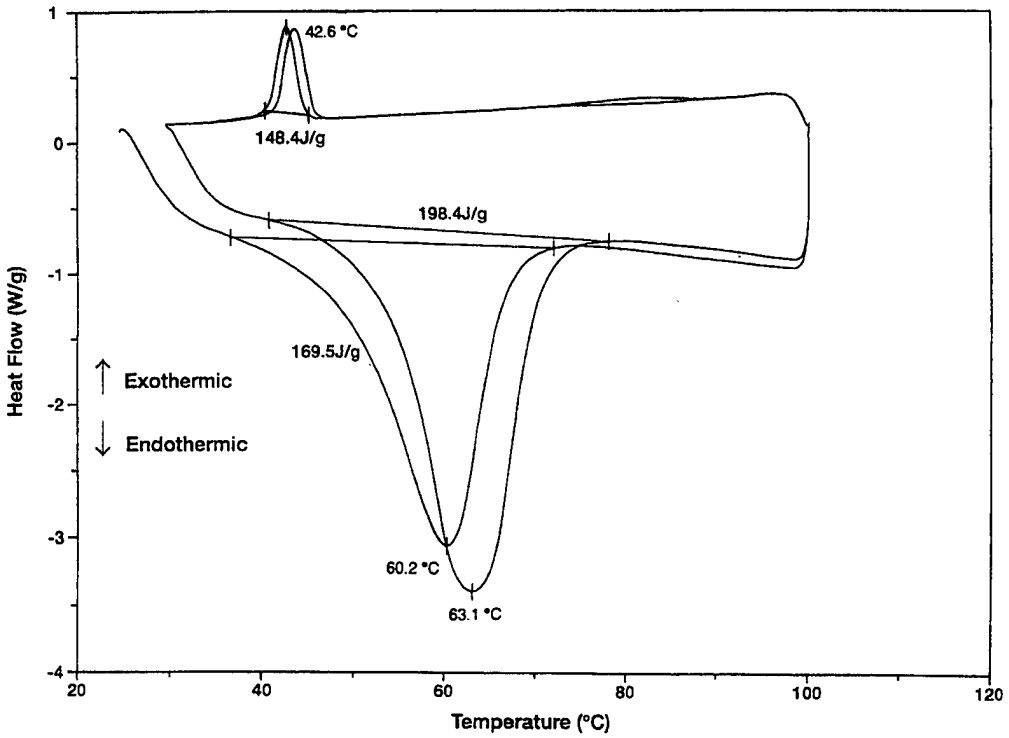


Figure 22. DSC Scans of PEO:$LiBF_4$ (8:1)-$Al_2O_3$ (20 wt%, 10 μm) Specimen

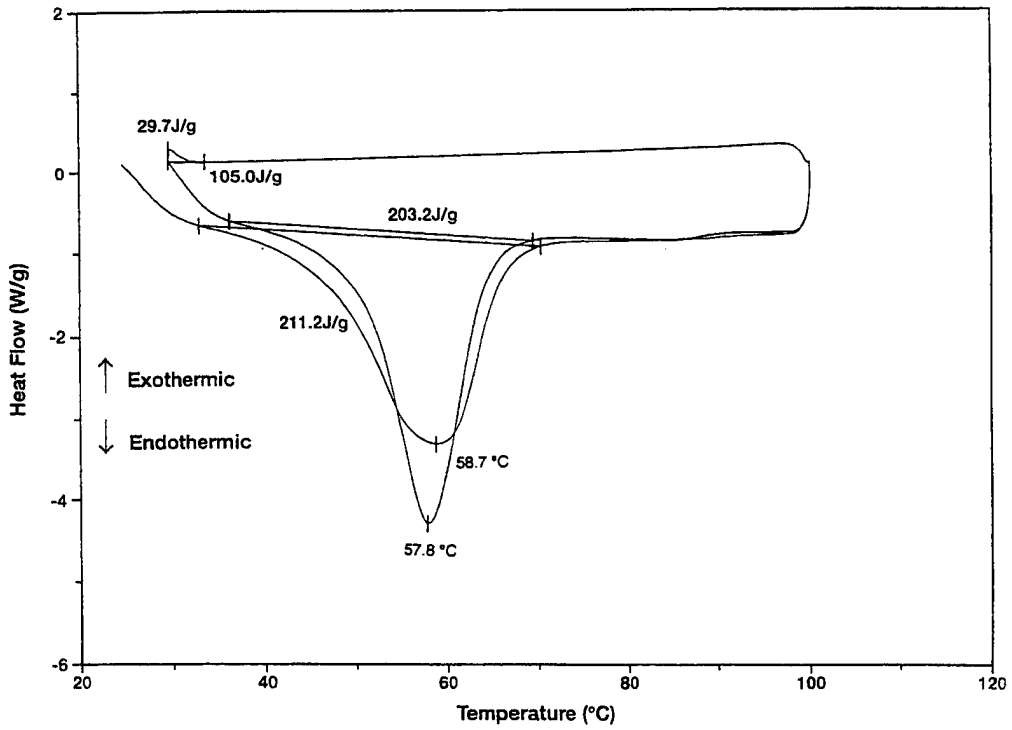


Figure 23. DSC Scans of PEO:$LiBF_4$ (8:1)-$Al_2O_3$ (20 wt%, 100 μm) Specimen

A recrystallization peak as evidenced by an exothermic peak during the cooling scan appears for the specimens containing particle sizes of 10 and 100 μm, as shown in Figures 22 and 23, respectively. For the 10 μm $Al_2O_3$ material, the recrystallization peak is located around 42.6 °C, whereas it shifts to 29.7 °C for the 100 μm $Al_2O_3$ material. Table 4 summarizes important observations obtained from the three specimens. It is apparent that nano-size (24 nm) $Al_2O_3$ is the most effective material in shifting the equilibrium of the crystalline ⇔ amorphous transition toward the right-hand side. In this case, the crystallinity is reduced by 46 percent during the second cycle and the amorphous phase remains stable during the cooling cycle, as there is no evidence of an exothermic peak in the DSC curve (Figure 21). There is a 17 percent enhancement in crystallinity during the second cycle in the specimen containing 10 μm $Al_2O_3$. The 100 μm $Al_2O_3$ specimen exhibits reduced (4 percent) crystallinity in the second cycle.

Table 4. Particle Size Effects on Crystallization of PEO:$LiBF_4$ (8:1)-$Al_2O_3$ (20 wt%) Material

| Particle Size | Endothermic Peak (1st Cycle) | | Endothermic Peak (2nd Cycle) | | Percent (%) Crystallinity | Exothermic Peak (1st Cycle) | |
|---|---|---|---|---|---|---|---|
| | Heat of Fusion, $Jg^{-1}$ | Peak Location, °C | Heat of Fusion, $Jg^{-1}$ | Peak Location, °C | Change | Heat of Fusion, $Jg^{-1}$ | Peak Location, °C |
| 24 nm | 221 | 60 | 119 | 51 | -46 | — | — |
| 10 μm | 169 | 60 | 198 | 63 | +17 | 148 | 43 |
| 100 μm | 211 | 59 | 203 | 58 | -4 | 105 | 30 |

The average length and mass of a PEO chain are 20 μm and 3 x $10^{-18}$ gm, respectively. These length and mass values of a PEO chain must now be compared with the particle size and mass of the ceramic dopant, $Al_2O_3$, to develop an insight into possible interactions. A constant segmental chain motion near the glass transition temperature is expected to cause displacement

and distribution of the $Al_2O_3$ particles. Furthermore, the process can be facilitated by thermal treatments and cycling. The displacement and distribution of $Al_2O_3$ particles continues until polymer chain dipole and $Al_2O_3$ dipole interaction takes place. The interaction leads to latching of the polymer chain and $Al_2O_3$ particle, and thus stabilization of the structure. When experimentally monitored, this phenomenon is reflected by an increase in conductivity during isothermal stabilization at low temperatures [12].

The degree of polymer chain and ceramic particle interaction can be reduced by incorporating $Al_2O_3$ particles having reduced surface-to-mass ratio. For example, if the weight percent of $Al_2O_3$ is maintained constant and the particle size is reduced from 5 μm to 24 nm, over 15 million additional polymer-ceramic interaction sites per unit volume are created and conductivity enhancements occur. As the particle size of $Al_2O_3$ is reduced from 100 μm to 24 nm, the mass of a particle is reduced by over 10 orders of magnitude. These lighter $Al_2O_3$ particles become far more receptive to the segmental chain motion of the polymer. As a result, improved polymer chain and $Al_2O_3$ particle interaction ensues. Such an interaction stabilizes the amorphous structure and imparts enhanced conductivity.

### 3.6 DIPOLES AND THEIR POSSIBLE EFFECTS

The dipoles are electrically active structural components in gases, liquids, and solids. The dipole and external electric field interaction is often quantified by a determination of the dielectric constant. The water molecule is a classic dipole which enables the liquid water to exhibit a high dielectric constant. The dipolar structure of the water molecule and its effects are retained even in ice [18].

The polymer electrolytes for applications in lithium rechargeable batteries have been investigated for two decades [1, 2], yet little is known and understood about their dipolar structure and its influence on conductivity. Takeuchi, et al. [19] have reported that 5 mole% of $BaTiO_3$ when dispersed in $Na_4Zr_2Si_3O_{12}$ increases its sodium ion conductivity. They attributed the conductivity enhancement to electrostatic forces originating from dipole moments of $BaTiO_3$ and subsequent increase in the hopping rate of the sodium ion. Sun, et al. [14, 20] also report enhancements in conductivity and lithium transport number of PEO:$LiClO_4$ when $BaTiO_3$ is added as a filler. The enhancements were due to spontaneous polarization of $BaTiO_3$.

The impetus for a proposal that dipoles exist in these composite electrolytes is driven by a long-term, reproducible, and consistent experimental observation that isothermal stabilization (annealing) of polymer (PEO:$LiBF_4$ complex)-ceramic (MgO, $TiO_2$, $ZrO_2$) composite electrolytes at a temperature near the melting point of PEO enhances conductivity. The conductivity enhancement may approach four orders of magnitude at subambient temperatures. The annealing time and cooling rate dependence of conductivity have been demonstrated in the PEO:$LiBF_4$-$TiO_2$ [21], PEO:$LiBF_4$-$ZrO_2$ [12], and PEO:$LiBF_4$-MgO [15] systems. It has been suggested [22] that thermally frozen, nonequilibrium, and randomly-oriented dipoles tend to approach an equilibrium, oriented configuration--a dipolar structure conducive for enhanced conductivity. The transition rate from a non-equilibrium to an equilibrium state is believed to be ceramic particle volume and size, and temperature dependent [22]. At low temperatures and for a larger volume fraction and particle size of ceramic phase, the time dependence of conductivity may be very small and may even be unobservable because the dipoles become immobile in a rigid polymer matrix.

The dipoles respond to electric field and mechanical force. Thus, appropriate experimental techniques to demonstrate the existence of dipoles must involve electrical and mechanical excitation and subsequent characterization. Under an applied dc field, the dipoles should orient in the direction of the field and subsequent measurement of conductivity using ac impedance should theoretically provide evidence of the physical presence of dipoles. Mechanical stretching leads to a change in molecular structure of the polymer and thus, an oriented dipolar configuration ensues. In view of the preceding background, we present results of an exploratory investigation with an objective to study the effects of dc field and mechanical stretching on conductivity. The underlying assumption is that the polymer-ceramic composite electrolytes are an assemblage of dipoles. These dipoles can be oriented under suitable conditions which in turn should influence the conductivity.

### 3.6.1 Conductivity Data of the Composite Electrolyte (without the dc field)

Conductivity data of composite electrolyte films obtained from PEO:$LiBF_4$ (8:1)-MgO (10 wt%) material are shown in Figure 7. A detailed discussion on their conductivity can be found in Section 3.2.2.

### 3.6.2 Effects of the dc Field

Figure 24 shows the temperature dependence of conductivity of the PEO:$LiBF_4$ (8:1)-MgO (10 wt%) composite electrolyte specimen with and without applied dc field. During a cooling scan, the specimen without an applied dc field was held at 20 °C for 16 hours and the conductivity increased by almost an order of magnitude – a situation similar to the results of Figure 7.

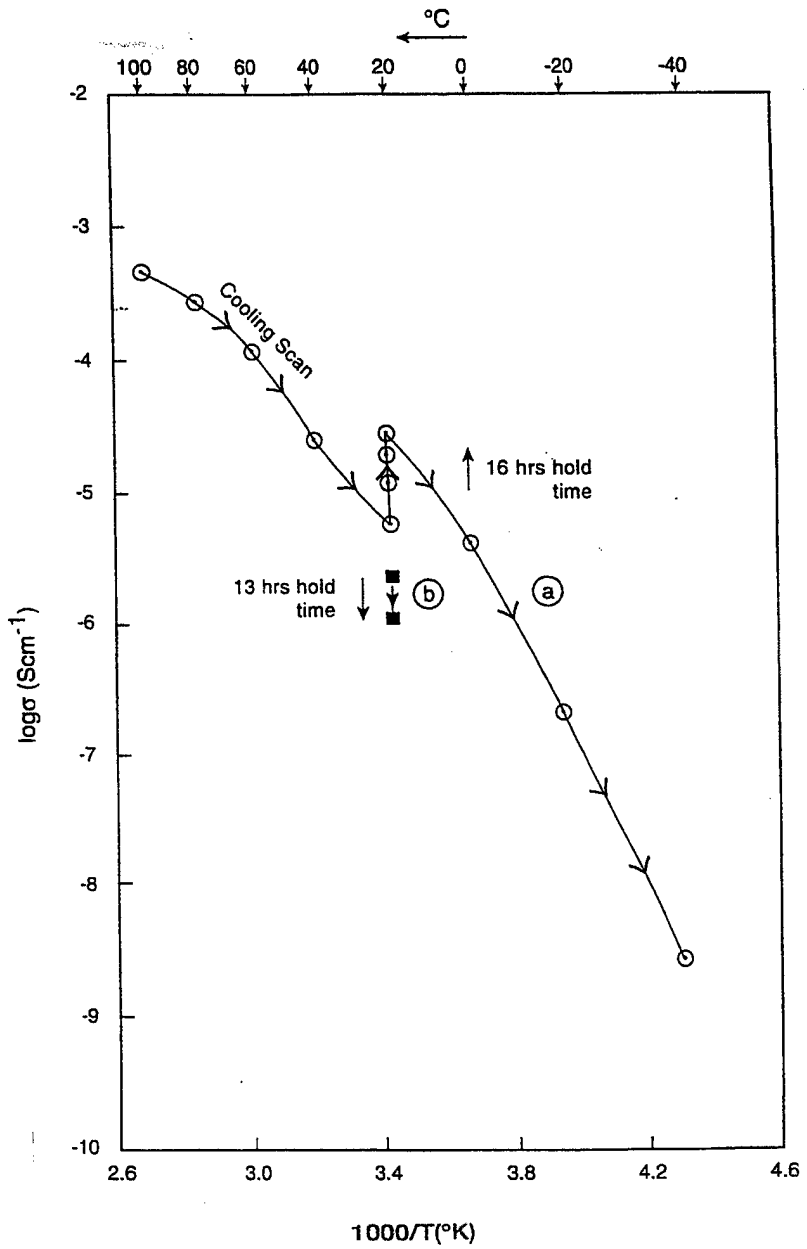


Figure 24. Conductivity of PEO:$LiBF_4$ (8:1)-MgO (10 wt%) Before and After Application of dc Field
(a) During Cooling Scan and Isothermal Stabilization at 20 °C, and
(b) Dc Field-Assisted, Rapidly Quenched Specimen Isothermally Stabilized at 20 °C

After the specimen was rapidly quenched under a dc field of 10 V $cm^{-1}$ from 100 to 20 °C, the measured conductivity (log $\sigma$ = -5.64) is lower than the value (log $\sigma$ = -5.24) obtained during the standard cooling scan by 33 percent. Although the dipoles have been aligned by the dc field, the lower conductivity of the dc field-assisted, rapidly-quenched specimen is attributed to polarization and depletion of ionic charge carriers. The interesting result to be noted here is that the isothermal stabilization of the specimen for 13 hours led to a further decrease in conductivity. This effect is attributed to a relative disorientation of dipoles driven by the thermal energy.

From the observations of this experiment, it is imperative that the active concentration of ionic charge carriers and orientation of dipoles are both affected by the dc field. The coupling of these two electrically-active species makes interpretation of the data a cumbersome task, and therefore other experimental techniques may have to be employed to study each of the electrically-active species.

### 3.6.3 Effect of Mechanical Stretching

When a solid assemblage of dipoles is subjected to a mechanical stress, each dipole is subjected to the stress in a localized manner and if a rotation of a dipole is allowed, an orientation of dipoles will take place and the conductivity will be affected.

The ac impedance spectra of a PEO:$LiCF_3SO_3$-MgO specimen prior to and after uniaxial mechanical stretching at 26 °C are shown in Figures 25(a) and (b), respectively. The measurement was conducted without any prior heat treatment of the films and represents a typical observation of the composite electrolytes. In general, specimens with no heat treatment

exhibit high resistance due to the presence of a crystalline phase. A comparison of the two spectra reveals that the resistance of the composite electrolyte after stretching decreased from $8 \times 10^6$ to $1.8 \times 10^6$ Ω. A reduction of the electrolyte resistance by a factor of almost five was achieved while the thickness of the film decreased by only 15 percent.

The temperature dependence of conductivity (inverse of resistance normalized by geometrical parameters of the film) data of the two specimens whose impedance data were presented in Figure 25 are shown in Figure 26. The cells containing these two specimens were contained in a glass vessel under controlled atmosphere. The two specimens were thermally stabilized and characterized simultaneously. The total thermal treatment time was 132 hours at 60 °C, which is believed to be sufficient to stabilize the structure of composite electrolytes. The conductivity measurement after thermal stabilization was initiated at 100 °C and terminated at 0 °C. In Figure 26, it is noted that in spite of the long annealing time, the conductivity of the stretched specimen remained about 40 percent greater than the unstretched specimen over the entire temperature range. Thus, the effect of mechanical stretching on conductivity is permanent and complements the effects rendered by isothermal stabilization leading to the formation of a predominantly amorphous structure.

Qualitatively, in low-yield stress material such as the polymers and composites used in this investigation, a higher level of stress will lead to a greater elongation of the film in the stretching direction. In these composite electrolytes, there is an optimum elongation ($\simeq$10 percent) beyond which the conductivity remains constant.

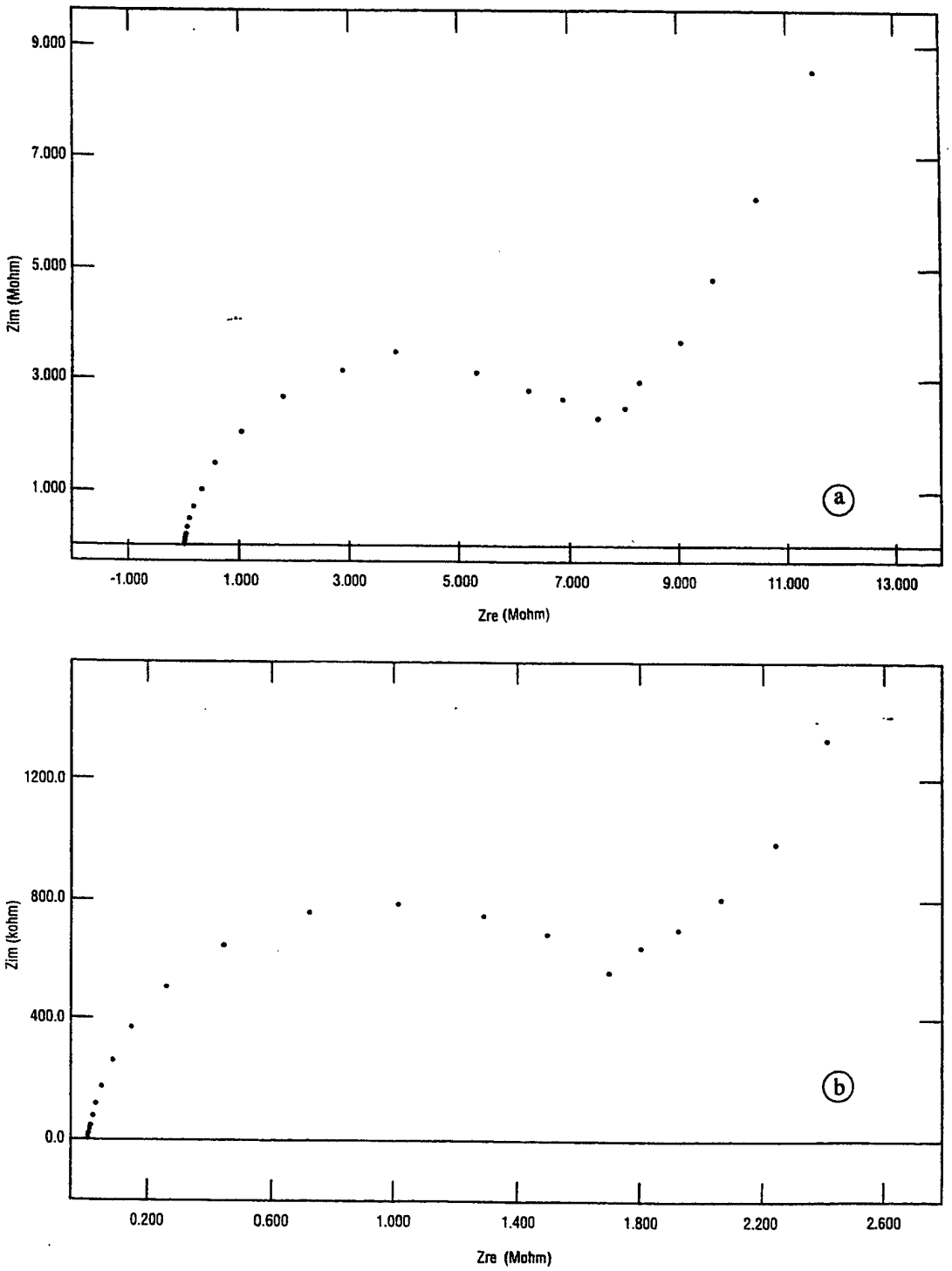


Figure 25. AC Impedance Spectra of PEO:$LiCF_3SO_3$ (8:1)-MgO (10 wt%) Films (a) As-Prepared and (b) After Stretching. The Specimen was Not Subjected to Any Prior Heat Treatment

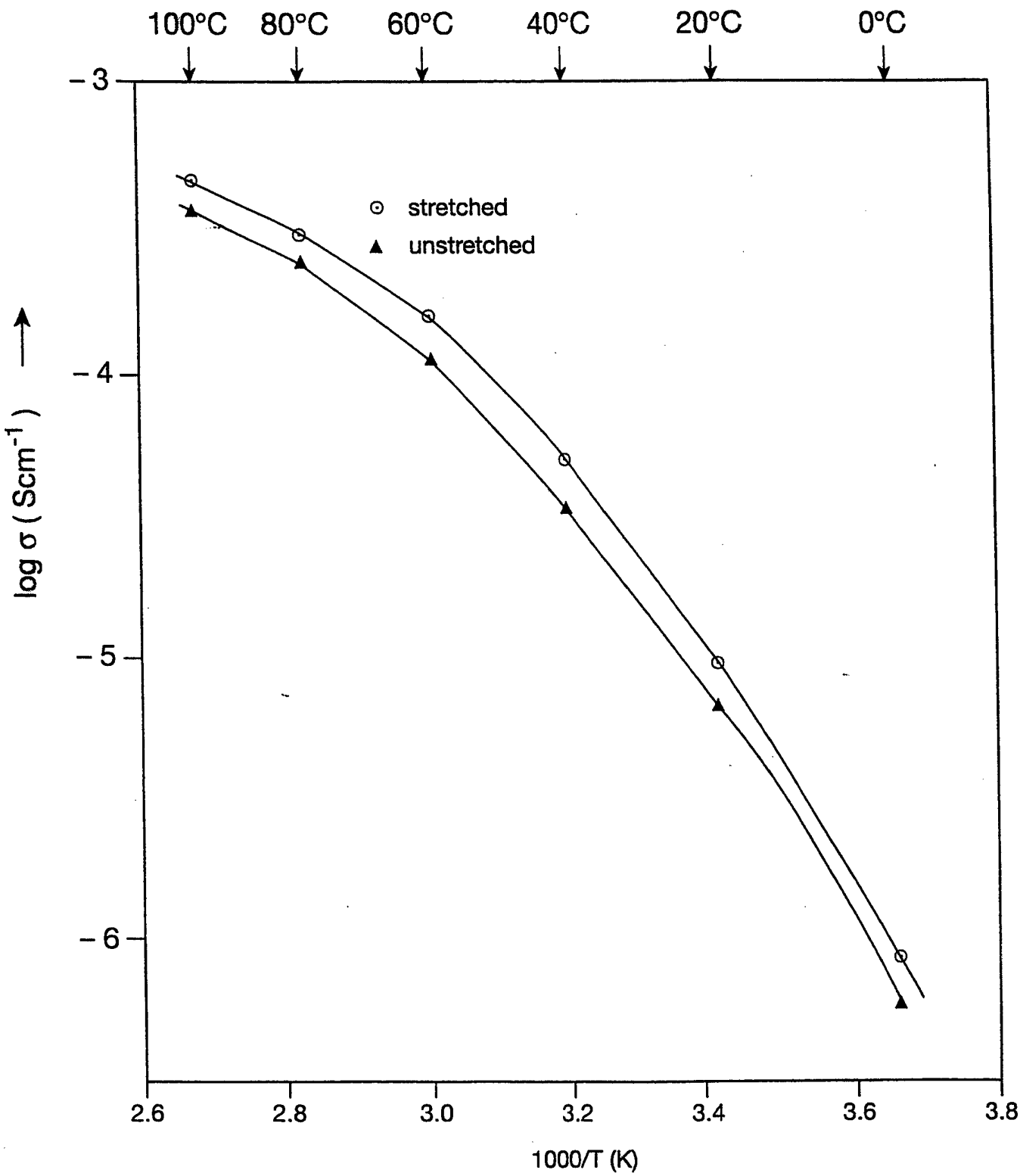


Figure 26. Temperature Dependence of Conductivity of PEO:$LiCF_3SO_3$ (8:1)-MgO (10 wt%) Films after Annealing at 60 °C for 132 Hours

### 3.6.4 Infrared Absorption Spectroscopy

The dielectric constants of PEO and MgO are 5 and 9.65, respectively. The dielectric constant gradient between the two phases raises a possibility of chemical interaction. Thus, the chemical bonds in the polymer complex (PEO:$LiBF_4$) are expected to be affected by the addition of MgO. These bonds may even be further influenced by an elongating stress. To explore and assess this possibility, the IR absorption spectra on as-prepared PEO:$LiBF_4$ (8:1) complex, PEO:$LiBF_4$ (8:1)-MgO (20 wt%) composite, and stretched PEO:$LiBF_4$ (8:1)-MgO (20 wt%) electrolyte films were obtained.

A comparison of IR spectra of as-prepared films of PEO:$LiBF_4$ (8:1) and PEO:$LiBF_4$ (8:1)-MgO (20 wt%) material are shown in Figure 27. Broad absorption in the 650 to 750 $cm^{-1}$ and bands in the 450 to 520 $cm^{-1}$ ranges result due to the addition of MgO. The absorption band at 528.4 $cm^{-1}$ in the PEO:$LiBF_4$ (8:1) complex is attributed to the bending mode of the (OCC) group [23]. With the addition of MgO in the complex, a chemical interaction takes place and additional bands appear at 514.8, 478.3, and 462.8 $cm^{-1}$. The 514.8 $cm^{-1}$ band may have resulted from a shift of the 528 $cm^{-1}$ band. Thus, it is evident that the addition of MgO leads to the formation of a ternary PEO:$LiBF_4$ (8:1)-MgO complex.

After a film of PEO:$LiBF_4$ (8:1)-MgO (20 wt%) was mechanically stretched, there are additional changes in the IR absorption spectra, as shown in Figure 28. The slope of the broad absorption in the 650 to 750 range increases and the individual bands shift by approximately 21 $cm^{-1}$ to higher frequencies. A slight shift in some other absorption bands also occurs which is summarized along with band assignments in Table 5. For reference, Table 5 also presents absorption bands associated with PEO as reported by Papke, et al. [23].

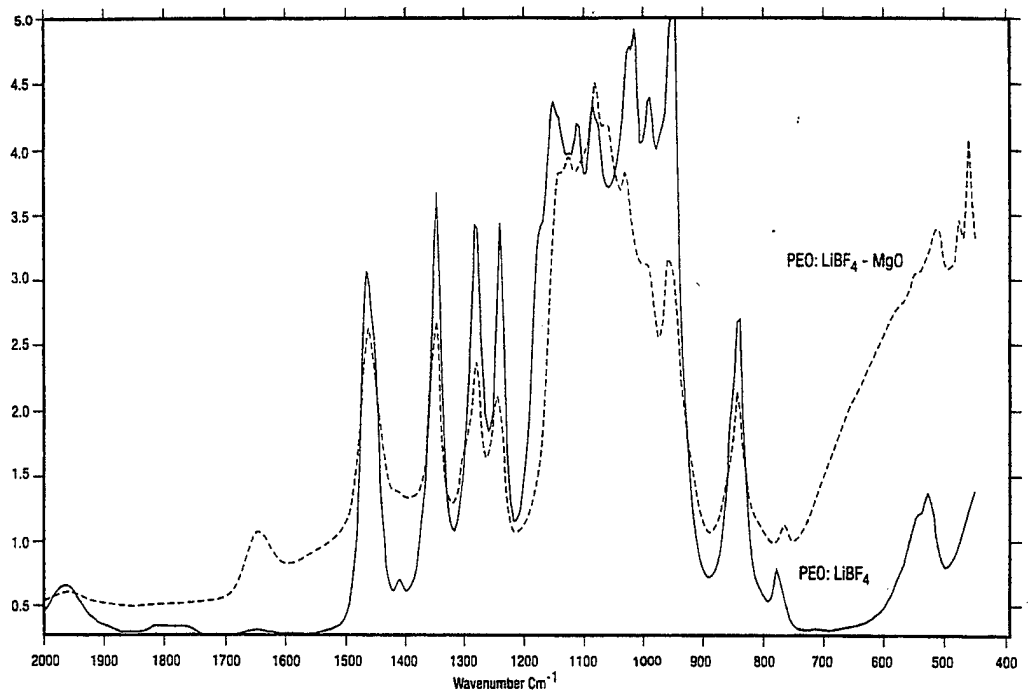


Figure 27. IR Absorption Spectra of PEO:$LiBF_4$ (8:1) Complex and PEO:$LiBF_4$ (8:1)-MgO (20 wt%) Composite Films

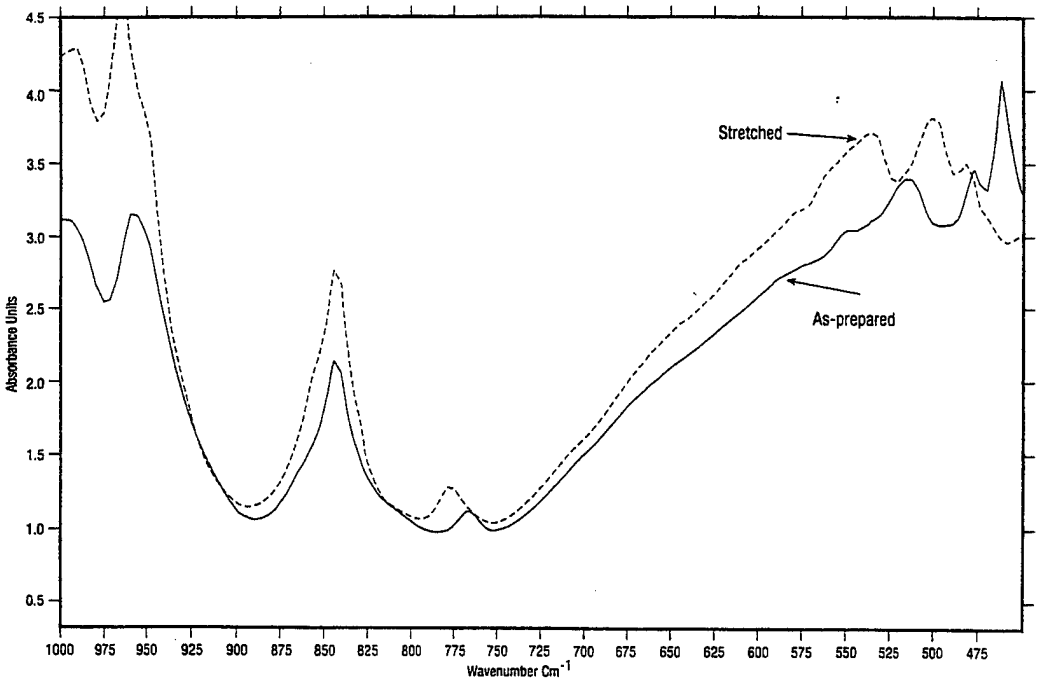


Figure 28. IR Absorption Spectra of PEO:$LiBF_4$ (8:1)-MgO (20 wt%) Composite Electrolyte Stretched and As-prepared

Table 5. Infrared Bands and Assignments in PEO:$LiBF_4$:MgO Complexes (2000 to 400 $cm^{-1}$)

| PEO | PEO:$LiBF_4$ (8:1) | PEO:$LiBF_4$-MgO (20 wt%) | | Assignments |
|---|---|---|---|---|
| | | Unstretched | Stretched | |
| 1960 | 1965.1 | 1961.4<br>1647.7 | 1965.8 | |
| 1473 | 1469.0 | 1466.8 | 1469.5 | $\delta$ $(CH_2)_a$ |
| 1342 | 1349.9 | 1349.9 | 1350.9 | $\omega$ $(CH_2)_a$ |
| 1283 | 1282.6 | 1281.6 | 1281.9 | t $(CH_2)_a$ |
| 1244 | 1241.9 | 1245.7 | 1241.9 | t $(CH_2)_a$ |
| 1147 | 1154.6 | 1128.7 | 1147.1 | |
| 1103 | 1113.0<br>1088.1<br>1017.9<br>992.4 | 1083.8<br>1033.0 | 1112.4<br>1097<br>1047<br>992.4 | $\nu$ $(COC)_a$ |
| 958 | 950.4 | 958.8 | 964.5 | r $(CH_2)_a$, $\nu$ $(COC)_a$ |
| 844 | 842.4<br>778.3 | 843.9<br>766.7 | 843.8<br>777.4 | r $(CH_2)_a$ |
| 530 | 528.4 | 514.8<br>478.3<br>462.8 | 536.1<br>500.4<br>482.4 | OCC–MgO $\delta(OCC)_a$<br>OCC-MgO<br>OCC-MgO |

r (rocking), t (twisting), $\nu$ (stretching), $\omega$ (wagging), $\delta$ (bending), a (asymmetric)

Chung, et al. [24] have conducted a nuclear magnetic resonance study on a film of PEO:LiI (20:1) and reported that short-range structural changes such as Li-H internuclear distances and local Li-O bond lengths and angles are affected when a uniaxial stress is applied. The structural changes are accompanied by reduced segmental chain motion of the host polymer.

Golodnitsky and Peled [25] reported a five-fold increase in conductivity of a PEO:LiI (20:1) specimen along the stretching direction when the specimen was mechanically stretched. They also observed development of fibrous morphology after stretching.

It is expected that the dipoles associated with polymer chain segment and MgO particles are aligned in the direction of stretching. However, the polymer chains are approximately 1,000 times larger than the MgO particles that may introduce additional bends and curvature in the long polymer chains. The polymer chains cross each other in the amorphous, bulk structure. An anisotropy of conductivity in the stretched specimen is a possibility that has not been characterized. This investigation presented and discussed conductivity data which has been measured perpendicular to the stretching direction.

## *SECTION 4*
## *SUMMARY AND CONCLUSIONS*

An analysis of a broader compositional range of composite electrolytes reveals that the incorporation of ceramic components in a PEO-based polymer matrix leads to enhanced conductivity. The processing of the composite electrolyte plays an important role. The conductivity enhancement varies depending upon the fraction of ceramic phase, annealing parameters, polymer-ceramic systems, and temperature. In some polymer-ceramic systems, an increase of approximately four orders of magnitude in conductivity around and below ambient temperature has been achieved. The enhancement is accompanied by a reduction in temperature dependence of conductivity. Analyses of experimental data strongly suggest that a new transport mechanism evolves. Specific conclusions of this investigation are as follows:

- The nano-size ceramic additives yield solid electrolytes with conductivities of about $10^{-4}$ S $cm^{-1}$ around ambient temperature. The micro-size additives yield about an order of magnitude lower conductivity at 20 °C and the difference widens as the temperature is lowered to -40 °C.
- The ceramic additives initially enhance conductivity by reducing the degree of crystallinity. Subsequently, polymer chain and ceramic particle interaction takes place which add to the magnitude of conductivity enhancement. The interaction is facilitated by reducing the particle size and mass of the ceramic particles. This interaction is also temperature and time dependent.
- The driving force for the polymer chain-ceramic interaction is the dielectric constant gradient; however, a larger difference in dielectric constant (such as use of $BaTiO_3$) adds little to the conductivity enhancement.

- The polymer phase remained the medium of transport and reservoir for conducting ions. The ceramic additives facilitated the transport of charge carriers through a localized influence on the polymer chain conformation.
- A reduction in the activation energy for the transport process resulting from a smaller size ceramic was attributed to a localized and asymmetric interaction induced by the ceramic particle.
- A thermal treatment at 175 °C of the melt cast specimen is an effective technique to eliminate the crystalline PEO phase. This temperature is well below the peak decomposition temperature of PEO.
- The particle size of the ceramic phase affects crystallization of the polymer phase. The nano-size ceramic was found to be the most efficient in eliminating the crystalline PEO phase and also in preventing its recrystallization.
- The composite electrolyte may be considered as an assemblage of permanent dipoles whose average orientation depends upon the temperature and prior thermal history of the specimen.
- The conductivity enhancement originates from an interaction of the dipoles associated with the polymer and ceramic phases.
- The conductivity of a specimen at 20 °C quenched under a dc field was lower and decreased further with isothermal stabilization. The lower conductivity was attributed to depletion of ionic charge carriers. The conductivity decay was linked to thermally-induced disorientation of dipoles.

- Absorption bands in the range of 460 to 530 $cm^{-1}$ develop as a result of MgO addition in the $PEO:LiBF_4$ complex. These bands shift to higher frequencies by approximately 21 $cm^{-1}$ due to stretching.

## *SECTION 5*
## *REFERENCES*


1. Polymer Electrolyte Reviews 1 and 2, edited by J. R. MacCallum and C. A. Vincent (Elsevier Applied Science Publishers Ltd., 1987).

2. F. M. Gray, Polymer Electrolytes, The Royal Society of Chemistry (1997).

3. K. Shahi, J. B. Wagner, and B. B. Owens, in Lithium Batteries, edited by J.-P. Gabano, Academic Press, New York (1983), p. 407.

4. C. A. Angell, *Solid State Ionics* 18 & 19, 72-88 (1986).

5. B. Kumar and L. G. Scanlon, *J. Power Sources* 52, 261-268 (1994).

6. E. Quartarone, P. Mustarelli, A. Magistris, *Solid State Ionics* 110, 1-14 (1998).

7. B. Kumar and L. G. Scanlon, *J. Electroceramics* 5:2, 127-139 (2000).

8. P. V. Wright, *Br. Polymer J.* 7, 319 (1975).

9. M. B. Armand, J. M. Chabagno, M. Duclot, in: P. Vashishta, et al. (Eds.), Fast Ion Transport in Solids (Elsevier, New York 1979), p. 131.

10. C. Berthier, W. Gorecki, M. Minier, M. B. Armand, J. M. Chabagno, and P. Rigand, *Solid State Ionics* 11, 91 (1983).

11. B. Kumar and J. Schaffer, WL-TR-95-2141 (1995).

12. B. Kumar and L. G. Scanlon, *Solid State Ionics* 124, 239-254 (1999).

13. P. G. Bruce, Polymer Electrolyte Reviews 1, 237-274 (Elsevier Applied Science Publishers Ltd., 1967).

14. H. Y. Sun, Y. Takeda, N. Imanishi, O. Yamamoto, H.-J. Sohn, *J. Electrochem. Soc.* 147(7), 2462-2467 (2000).

15. B. Kumar, L. Scanlon, R. Marsh, R. Mason, R. Higgins, and R. Baldwin, *Electrochimica Acta* 46, 1515-1521 (2001).

16. A. R. VonHippel, Dielectric Materials and Applications, The M.I.T. Press, p. 38 (1954).

17. B. Kumar, S. J. Rodrigues, and L. G. Scanlon, to be published in *J. Electrochem. Soc.* (2001).

18. P. Debye, Polar Molecules, Dover Publications, New York, pp. 102-104 (1945).

19. T. Takeuchi, K. Ado, Y. Saito, M. Tabuchi, H. Kageyama, and O. Nakamura, *Solid State Ionics*, 89, 345-349 (1996).

20. H. Y. Sun, H.-J. Sohn, O. Yamamoto, Y. Takeda, and N. Imanishi, *J. Electrochem. Soc.* 146(5), 1672-1676 (1999).

21. B. Kumar and L. G. Scanlon, SAE Aerospace Power Systems Conference, Williamsburg, VA, 71-82 (April 9-11, 1997).

22. B. Kumar, L. G. Scanlon, and R. J. Spry, *Journal of Power Sources, 96/2, 337-342* (2001).

23. B. L. Papke, M. A. Ratner, D. F. Shriver, *J. Electrochem. Soc.* 129(7), 1434-1438 (1982).

24. S. H. Chung, Y. Wang, S. G. Greenbaum, D. Golodnitsky, and E. Peled, *Electrochem. Solid State Lett.* 2(11), 553-555 (1999).

25. D. Golodnitsky and E. Peled, *Electrochemica Acta* 45, 1431-1436 (2000).

## *LIST OF SYMBOLS AND ACRONYMS*

### List of Symbols:

$b$ = distance between potential wells for dipolar interaction, m

$b_i$ = distance between potential wells for ionic conduction, m

$e$ = electron charge, C

$\Delta E$ = activation energy, k J $mol^{-1}$

$G$ = shear modulus, GPa

$k$ = Boltzmann constant, $10^{-23}$ J $K^{-1}$

$n$ = number of dipoles, dimensionless

$n'$ = number of charge carriers, dimensionless

$P$ = polarization, $m^3$

$R$ = gas constant, 8.314 J $mol^{-1}$ $k^{-1}$

$r$ = radius of the conducting ion, m

$r_D$ = doorway radius, m

$r_o$ = radius of the oxygen ion, m

$T$ = temperature, K

$v$ = covalency parameter, dimensionless

$z$ = valence of conducting ions, dimensionless

$z_o$ = valence of oxygen ion, dimensionless

Greek

$\alpha$ = accommodation coefficient, dimensionless

$\beta$ = displacement factor, dimensionless

$\kappa$ = dielectric constant, dimensionless

$\mu$ = mobility, $m^2v^{-1}s^{-1}$

$\nu_j$ = relaxation frequency ($1/\tau_j$), $s^{-1}$

$\nu'$ = vibrational frequency of charge carriers, $s^{-1}$

$\sigma_j$ = relaxation amplitude, S $cm^{-1}$

$\sigma(\infty)$ = equilibrium conductivity, S $cm^{-1}$

$\sigma'(t)$ = conductivity at time t (s), S $cm^{-1}$

$\tau_j$ = relaxation time, s

Subscript

i = ionic specie

m = micrometer size

n = nanometer size

### List of Acronyms:

| | |
|---|---|
| AFRL/PRPS | Air Force Research Laboratory Energy Storage and Thermal Sciences Branch |
| DSC | Differential Scanning Calorimetry |
| FTIR | Fourier Transform Infrared |
| IR | Infrared |
| PEO | Poly(ethylene oxide) |